EP711 Introduction: *Modeling and Simulation*

Jonathan B. Snively
Embry-Riddle Aeronautical University

Experimental Science (The Science Fair perspective.)

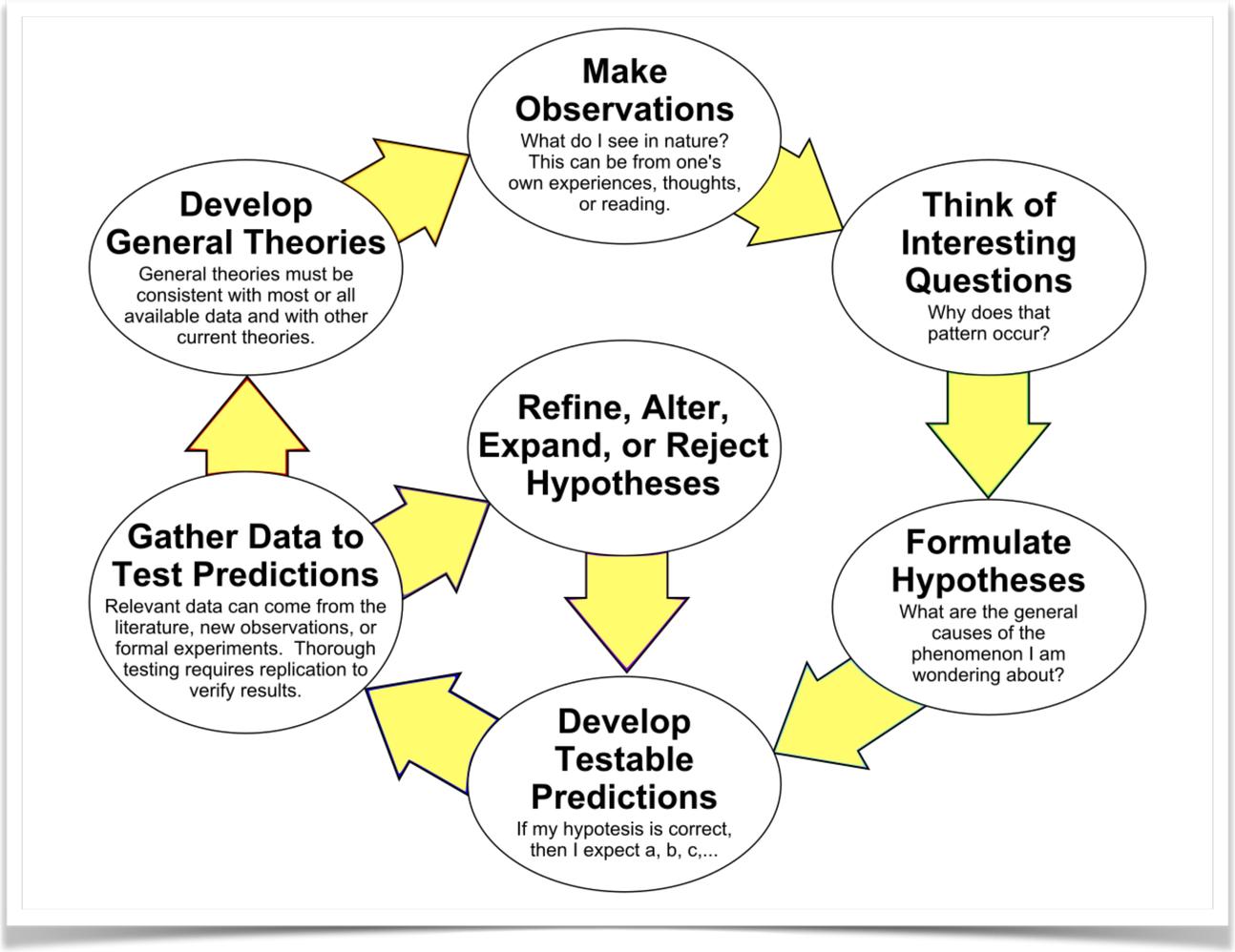

[https://en.wikipedia.org/wiki/Scientific_method#/media/File:The_Scientific_Method_as_an_Ongoing_Process.svg]

Experimental Science (Ignoring the role of models.)

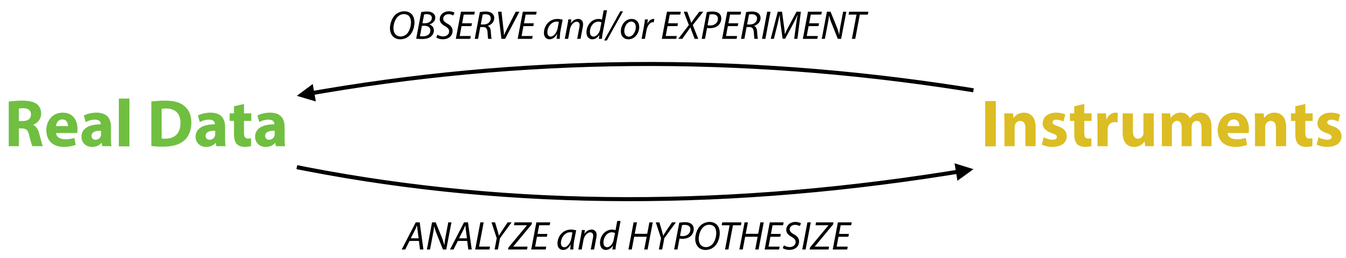

Experimental Science (Ignoring the role of models.)

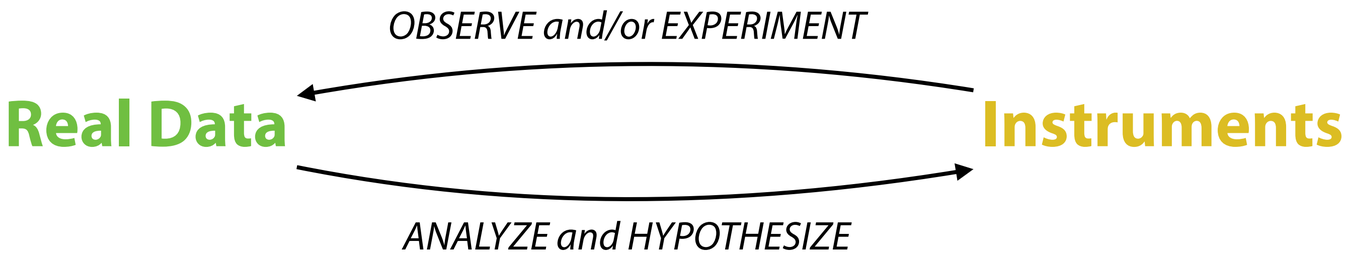

*Iterate until results ≥ 1LPU**

Experimental Science (Ignoring the role of models.)

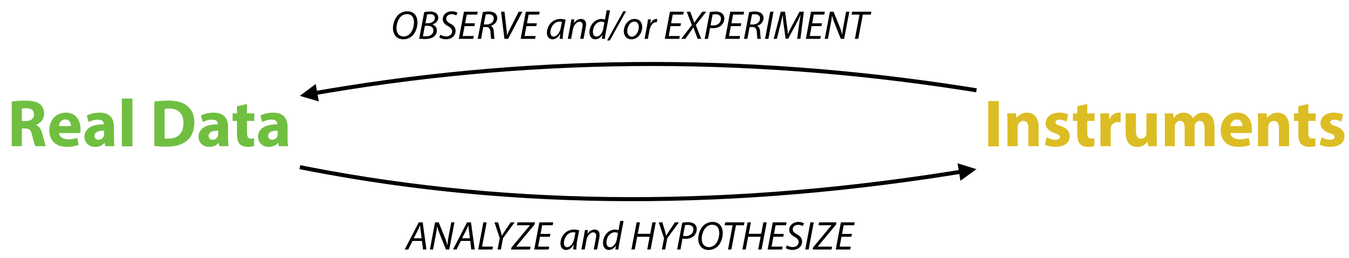

*Iterate until results ≥ 1LPU**

**LPU = "Least Publishable Unit"*

Experimental Science (Ignoring the role of models.)

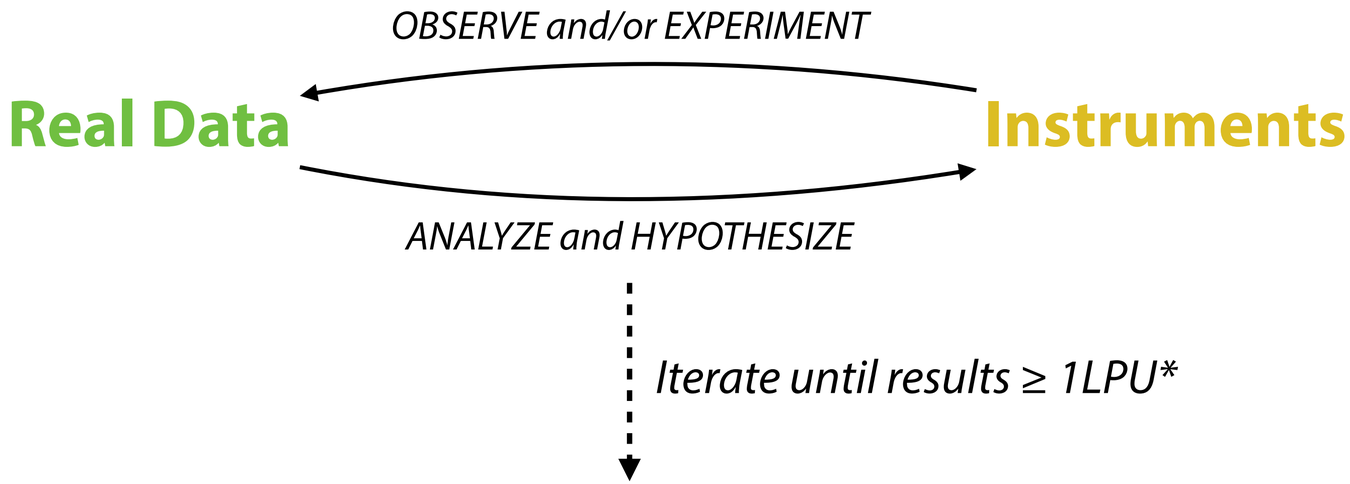

*LPU = "Least Publishable Unit"

Experimental Science (Ignoring the role of models.)

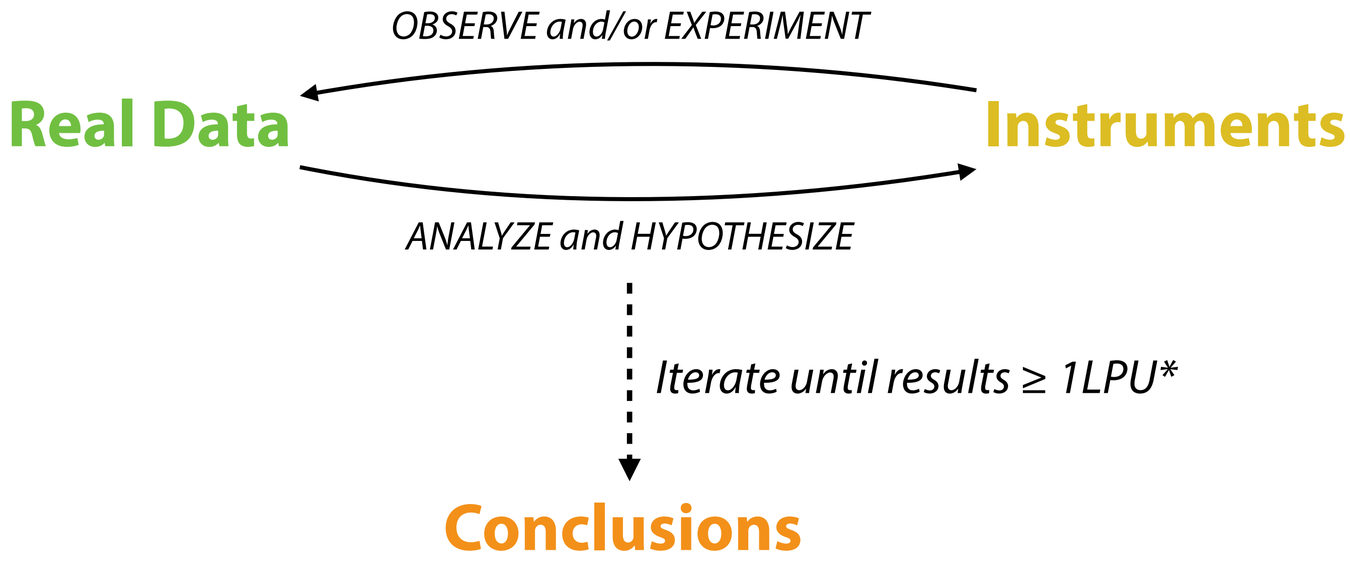

*LPU = "Least Publishable Unit"

Experimental Science (Ignoring the role of models.)

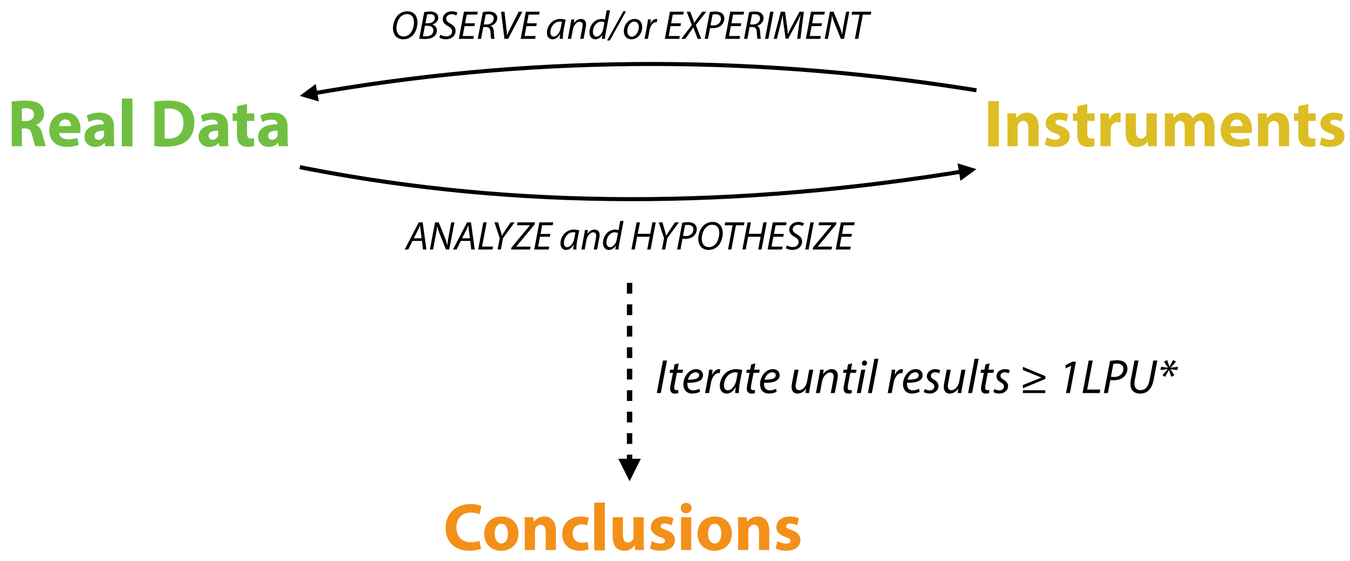

In Physics, "Conclusions" are often *useful mathematical relationships*, e.g., "Mathematical Models", which may (upon thorough testing) become "Laws" (Predictive/Descriptive), or which may inspire "Theories" (Explanatory).

**LPU = "Least Publishable Unit"*

Experimental Science

(As a model matures,
it can join in the loop.)

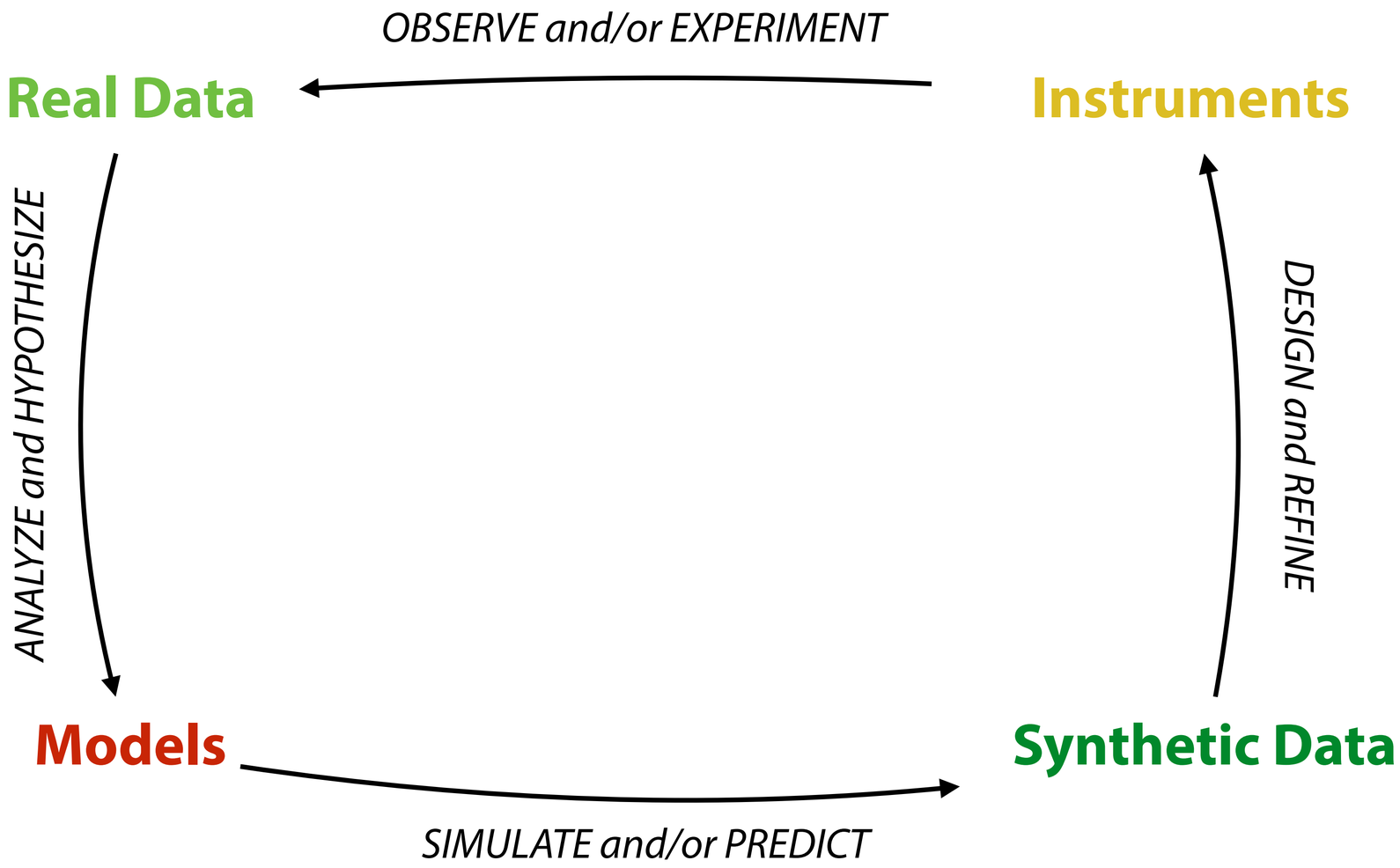

Experimental Science

(As a model matures,
it can join in the loop.)

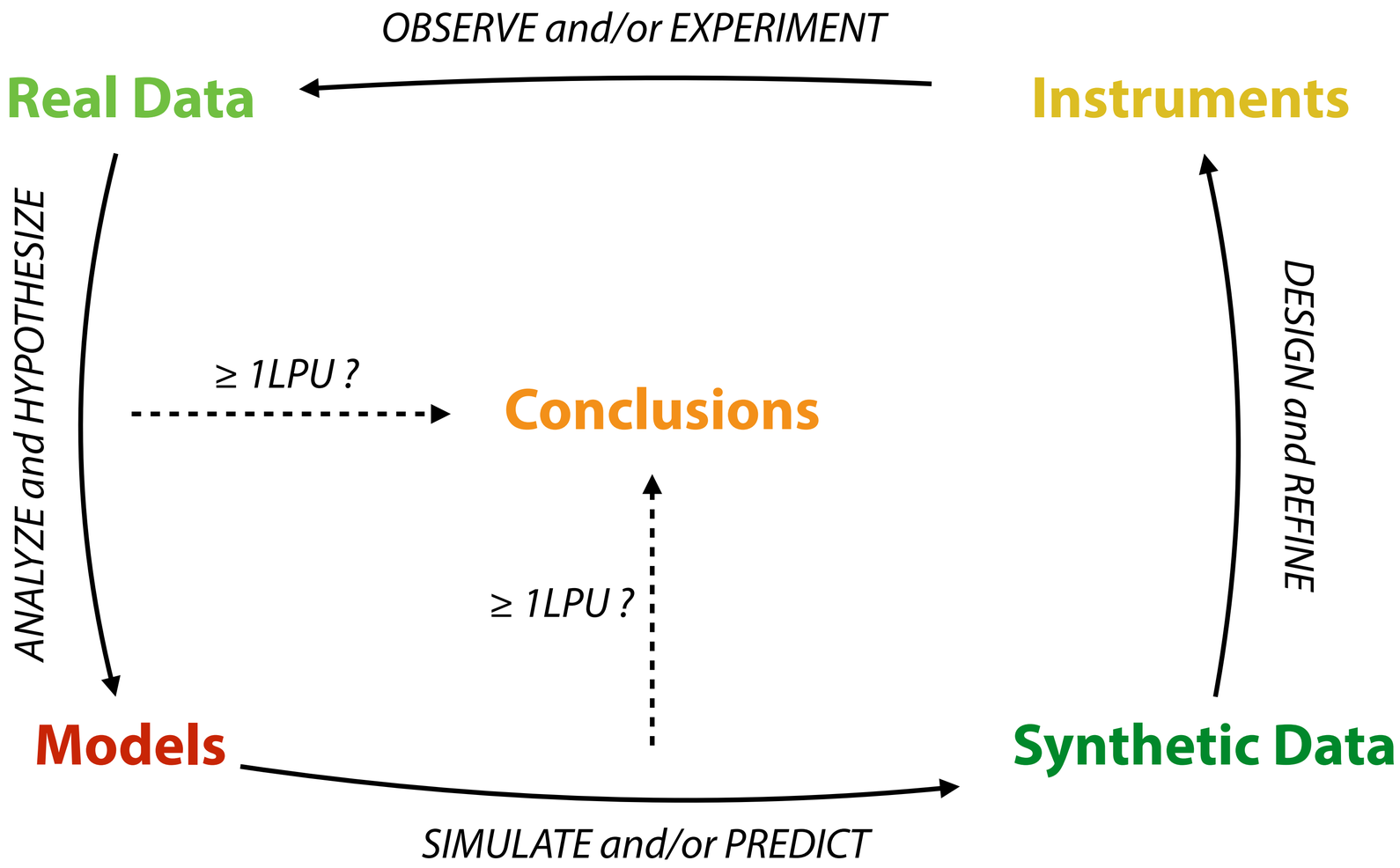

Multiple Roles for Models

- To *explain data* (experimental or observational), via case studies.
- To *test theories/hypotheses*, by simulating processes that are too complicated or nonlinear to describe analytically.
- To *fill in the gaps*, where observations are simply not feasible.
- To *simulate scenarios*, that could hypothetically be observed, i.e., to generate synthetic data to guide future experiments.
- To *enhance their validation*, to the extent necessary to predict or forecast outcomes, often with input from data. (May be a step towards Operations.)

What we call "Models" in Aeronomy and Space Physics

- *Mathematical* Models, based on Physical Laws and Theory*.
- *Physics-Based* Numerical Models, numerical solutions to Mathematical Models that are based on Physical Theory.
- *Empirical /* Statistical Models, based on fits to Data.
- Physics + *Assimilation* Models, which combine Physics-Based Numerical Models with active constraints by Data.

**which typically have empirical origins from Data, too.*

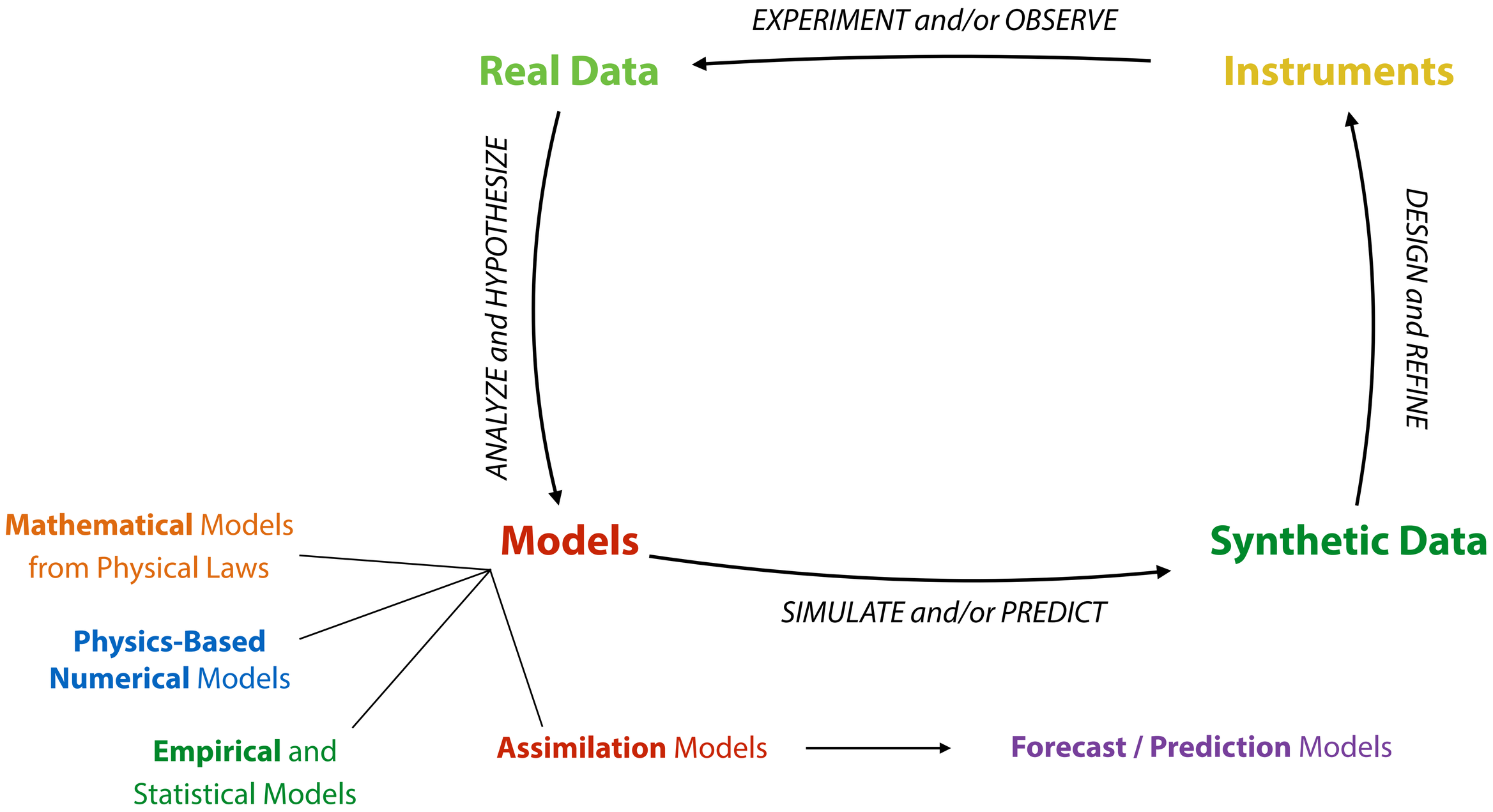
EXPERIMENT and/or OBSERVE
Real Data
Instruments
ANALYZE and HYPOTHESIZE
DESIGN and REFINE
Mathematical Models from Physical Laws
Physics-Based Numerical Models
Empirical and Statistical Models
Models
Synthetic Data
SIMULATE and/or PREDICT
Assimilation Models
Forecast / Prediction Models

Mathematical Models

Model physical processes within certain limits, e.g., “laws”, “governing equations”.

Newton’s Law

$$\mathbf{F} = m\mathbf{a}$$

Ohm’s Law

$$\mathbf{J} = \sigma\mathbf{E}$$

Mathematical Models

Model physical processes within certain limits, e.g., “laws”, “governing equations”.

Navier-Stokes Equations

$$\frac{\partial \rho}{\partial t} + \nabla \cdot (\rho \mathbf{v}) = 0$$

$$\frac{\partial}{\partial t}(\rho \mathbf{v}) + \nabla \cdot (\rho \mathbf{v}\mathbf{v} + p\mathbf{I}) = \rho \mathbf{g} + \nabla \cdot \boldsymbol{\tau}$$

$$\frac{\partial E}{\partial t} + \nabla \cdot \{(E + p)\mathbf{v}\} = \rho \mathbf{g} \cdot \mathbf{v} + (\nabla \cdot \boldsymbol{\tau}) \cdot \mathbf{v} + \kappa \nabla^2 T$$

$$E = \rho \epsilon + \frac{1}{2}\rho(\mathbf{v} \cdot \mathbf{v})$$

$$\tau_{ij} = \mu \left(\frac{\partial v_i}{\partial x_j} + \frac{\partial v_j}{\partial x_i} - \frac{2}{3}\delta_{ij} \frac{\partial v_k}{\partial x_k} \right)$$

Maxwell Equations

$$\nabla \cdot \mathbf{D} = \rho$$

$$\nabla \cdot \mathbf{B} = 0$$

$$\nabla \times \mathbf{E} = -\frac{\partial \mathbf{B}}{\partial t}$$

$$\nabla \times \mathbf{H} = \mathbf{J} + \frac{\partial \mathbf{D}}{\partial t}$$

$$\mathbf{D} = \epsilon \mathbf{E}$$

$$\mathbf{H} = \frac{1}{\mu}\mathbf{B}$$

Mathematical Models of Physics

Used frequently in Aeronomy / Space Physics.

- Equations for ray-tracing / trajectories of waves / particles.
- Equations of continuous fluid motion: Euler, Navier-Stokes.
- Equations of gas kinetics / statistical mechanics.
- Maxwell's equations of electromagnetics / electrodynamics.
- The magnetohydrodynamic (MHD) equations.
- Multi-fluid plasma dynamics equations.
- Chemical reaction equations + kinetics + transport.

Physics-Based Numerical Models

Used frequently in Aeronomy / Space Physics.

- Equations for ray-tracing / trajectories of waves / particles.
- Equations of continuous fluid motion: Euler, Navier-Stokes.
- Equations of gas kinetics / statistical mechanics.
- Maxwell's equations of electromagnetics / electrodynamics.
- The magnetohydrodynamic (MHD) equations.
- Multi-fluid plasma dynamics equations.
- Chemical reaction equations + kinetics + transport.

Physics-Based Numerical Models

Used frequently in Aeronomy / Space Physics.

Numerical Solutions to:

- Equations for ray-tracing / trajectories of waves / particles.
- Equations of continuous fluid motion: Euler, Navier-Stokes.
- Equations of gas kinetics / statistical mechanics.
- Maxwell's equations of electromagnetics / electrodynamics.
- The magnetohydrodynamic (MHD) equations.
- Multi-fluid plasma dynamics equations.
- Chemical reaction equations + kinetics + transport.

Physics-Based Numerical Models

Always limited by:

- Their underlying mathematical model and its physical basis.
- Their underlying numerical solution techniques.

And also limited by:

- Domain grid(s) / mesh(es), coordinate system(s), boundary conditions.
- Assumptions of linearity vs. nonlinearity; time-dependence vs. steady-state.
- Assumptions about sources, sinks, free parameters, initial conditions (data!).
- Interfaces (coupling) with *other* models (Empirical, Assimilation, etc.).
- The computational cost to achieve a desired resolution, scale, or runtime.

Examples: **WACCM CMAM SWMF GITM**
TGCM / TIE- / TIME-GCM
MM5 WRF SAMI 2/3

Empirical Models

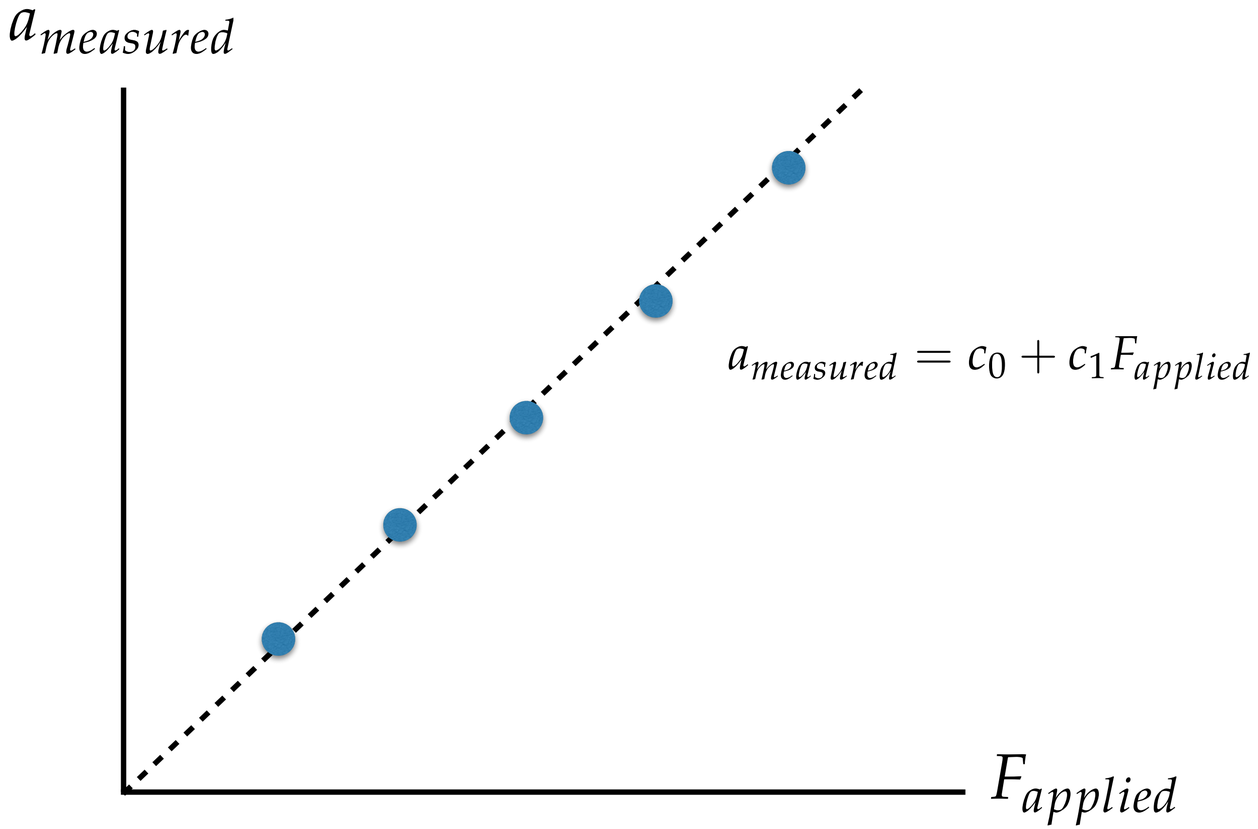

- *New* empirical models are validated through their agreement with data and mathematical/physical models.
  (Does c_1=m^{-1}? Is c_0~0? Are errors ~minimized?)
- *Established* empirical models can provide validation for mathematical/physical models. They capture trends that may evince physical laws.
  (Does F=ma?)

Examples: **MSISE-90 / NRLMSISE-00**
HWM-93 / -07 / -14 IRI CIRA

Assimilation Models

In Aeronomy and Space Physics, trusted Empirical Models routinely provide data as "context" for Physics-Based Numerical Model simulations.

Assimilation Models integrate active updates from measurements with a Physics-Based Numerical Model to enable **forecasts** and **predictions**.

Examples:

ECMWF / IFS / EULAG
WACCM-DART
CTIPe
USU-GAIM JPL-GAIM
NAVGEM / NAVDAS-AR
WRF / WRFDA

Let's look at some *specific* recent examples of Physics-Based Modeling to explain theory or observations.

JOURNAL OF GEOPHYSICAL RESEARCH, VOL. 90, NO. D2, PAGES 3850–3868, APRIL 20, 1985

The Effect of Breaking Gravity Waves on the Dynamics and Chemical Composition of the Mesosphere and Lower Thermosphere

ROLANDO R. GARCIA

National Center for Atmospheric Research, Boulder, Colorado

SUSAN SOLOMON

NOAA/Aeronomy Laboratory, Boulder, Colorado

The influence of breaking gravity waves on the dynamics and chemical composition of the 60- to 110-km region has been investigated with a two-dimensional dynamical/chemical model that includes a parameterization of gravity wave drag and diffusion. The momentum deposited by breaking waves at mesospheric altitudes reverses the zonal winds, drives a strong mean meridional circulation, and produces a very cold summer and warm winter mesopause, in general agreement with observations. The seasonal variations of the computed eddy diffusion coefficient are consistent with the behavior of mesospheric turbulence inferred from MST radar echoes. In particular, it is found that eddy diffusion is strong in summer and winter but much weaker at the equinoxes and that this seasonal behavior has important consequences for the distribution of chemical species. Comparison between computed atomic oxygen and ozone, and the abundances of these constituents inferred from the 557.7-nm and 1.27-μm airglow emissions, reveals excellent agreement. The consistency between model results and these diverse types of observations lends strong support to the hypothesis that gravity waves play a very important role in determining the zonally averaged structure of the mesosphere and lower thermosphere.

Oxygen and Ozone Airglow from Model vs. Satellite Da

Model Confirmation of GW effects on summer/winter mesopause temperature.

[*Garcia and Solomon*, JGR, 90, 1985]

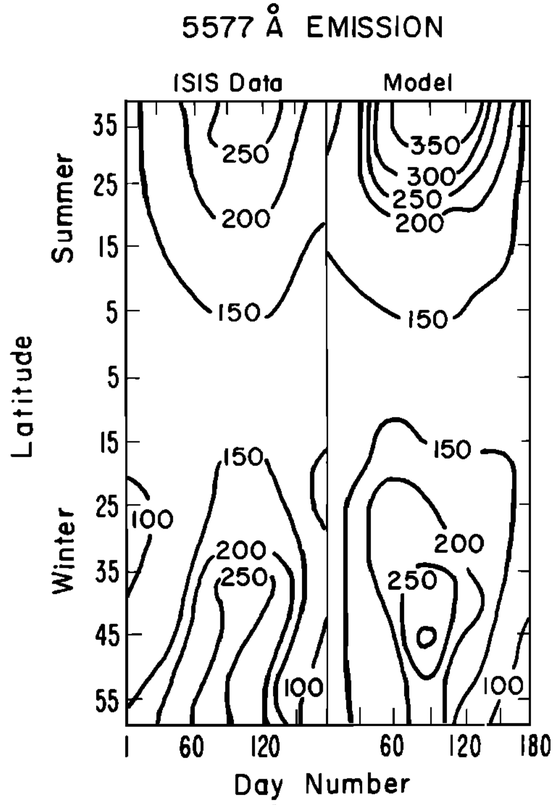

Fig. 15. Seasonal and latitudinal variations of atomic oxygen O green line emission intensities as observed by the ISIS satellite [*Cogger et al.*, 1981] and calculated in the model. Data and model results labeled "summer" ("winter") encompass the spring (fall) maximum. See Cogger et al. for details.

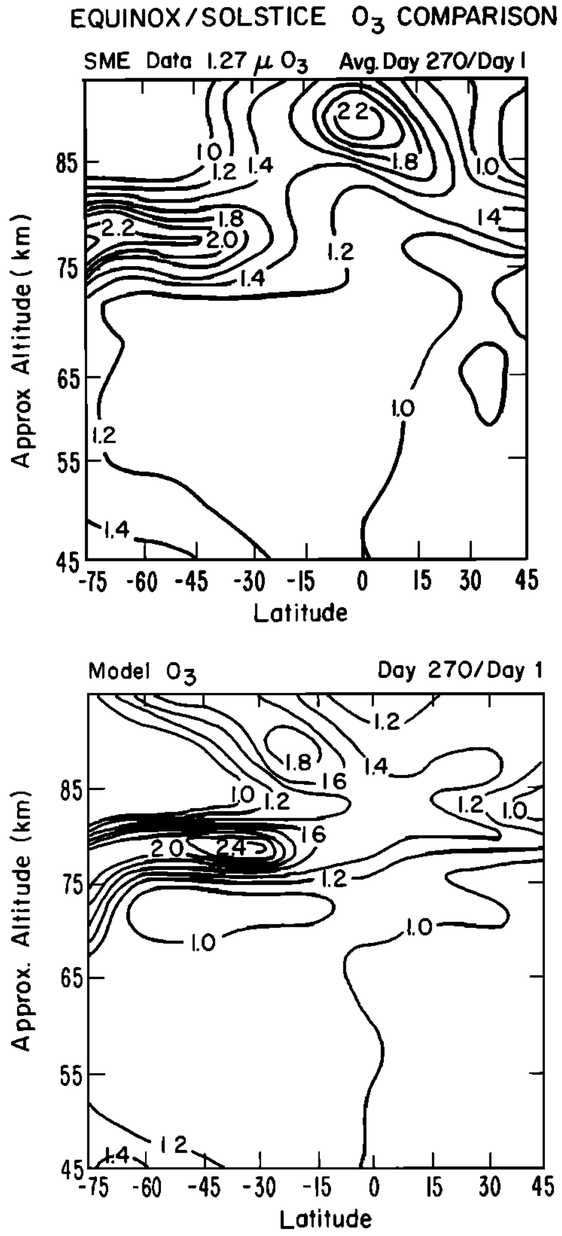

Fig. 18. (Top) Ratio of O_3 observations by the Solar Mesosphere Explorer satellite [*Thomas et al.*, 1984] for 1-week averages about day 270 to day 1 (southern hemisphere spring/summer; northern hemisphere fall/winter). (Bottom) Same, as computed by the model.

GEOPHYSICAL RESEARCH LETTERS, VOL. 20, NO. 19, PAGES 2039-2042, OCTOBER 8, 1993

WAVE BREAKING SIGNATURES IN NOCTILUCENT CLOUDS

David C. Fritts, Joseph R. Isler, and Gary E. Thomas
Laboratory of Atmospheric and Space Physics, University of Colorado

Øyvind Andreassen
Norwegian Defense Research Establishment

Abstract. Results of a recent modeling study of gravity wave breaking in three dimensions by *Andreassen et al.* and *Fritts et al.* showed wave saturation to occur via a three-dimensional instability oriented normal to the direction of wave propagation. The instability was found to occur at horizontal scales comparable to the depth of unstable regions within the wave field and to lead to substantial vertical displacements and tilting of isentropic surfaces. Because of strong similarities between the wave and instability structures in the simulation and the structure observed in noctilucent cloud layers near the summer mesopause, we have used these model results to compute the advective effects on cloud visibility and structure for a range of viewing angles and cloud layer widths. Our results show the gravity wave breaking signature to provide a plausible explanation of the observed structures and suggest that noctilucent cloud structures may be used in turn to infer qualitative properties of gravity wave scales, energy and momentum transports, and turbulence scales near the summer mesopause.

Wave-Driven Instabilities in Noctilucent Clouds

[*Fritts et al.*, GRL, 20, 1993]

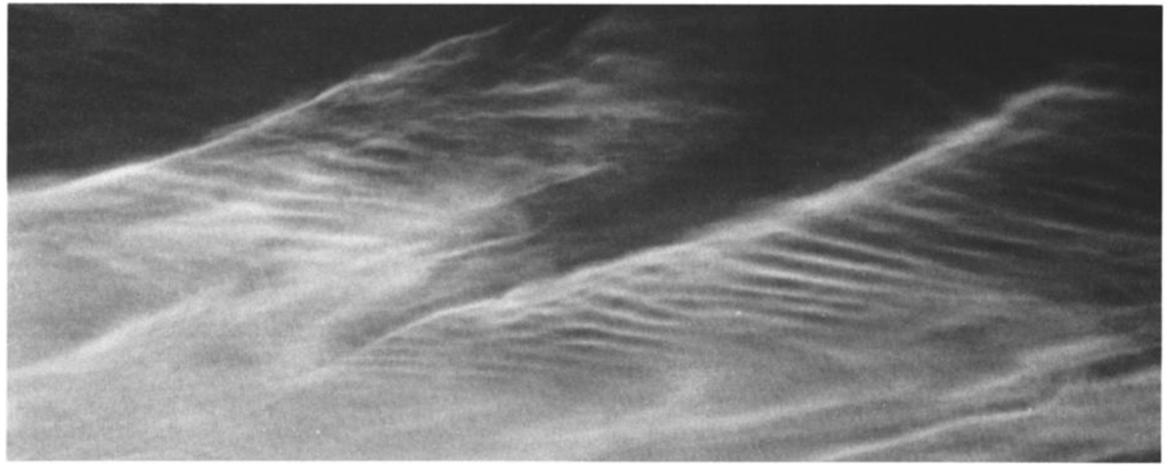

Figure 1. View of NLC display from Kustavi, Finland (61°N, 21°E) on 22 July 1989 showing characteristic band and streak structures. In this case, bands are separated by ~ 50 *km* and streaks by ~ 3 to 5 *km* (photo by Pekka Parviainen).

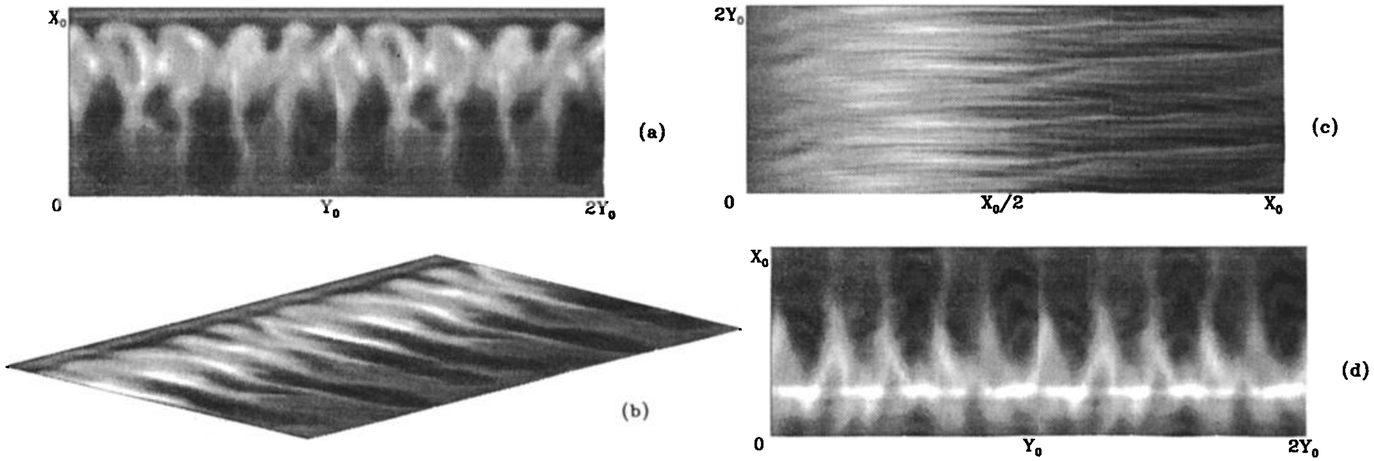

Figure 2. Simulated NLC brightness at the time of maximum instability amplitude at an elevation of 18° and azimuths of 180° (a), 135° (b), 90° (c), and 0° (d). These images represent projections of an area with $x_0 = 2y_0 = 4H$.

Available online at www.sciencedirect.com
ScienceDirect
Journal of Computational Physics 227 (2008) 3465–3485
JOURNAL OF COMPUTATIONAL PHYSICS
www.elsevier.com/locate/jcp

A time-split nonhydrostatic atmospheric model for weather research and forecasting applications

William C. Skamarock *, Joseph B. Klemp

National Center for Atmospheric Research,[1] P.O. Box 3000, Boulder, CO, 80307-3000, USA

Received 6 July 2006; received in revised form 24 January 2007; accepted 25 January 2007
Available online 17 February 2007

Abstract

The sub-grid-scale parameterization of clouds is one of the weakest aspects of weather and climate modeling today, and the explicit simulation of clouds will be one of the next major achievements in numerical weather prediction. Research cloud models have been in development over the last 45 years and they continue to be an important tool for investigating clouds, cloud-systems, and other small-scale atmospheric dynamics. The latest generation are now being used for weather prediction. The Advanced Research WRF (ARW) model, representative of this generation and of a class of models using explicit time-splitting integration techniques to efficiently integrate the Euler equations, is described in this paper. It is the first fully compressible conservative-form nonhydrostatic atmospheric model suitable for both research and weather prediction applications. Results are presented demonstrating its ability to resolve strongly nonlinear small-scale phenomena, clouds, and cloud systems. Kinetic energy spectra and other statistics show that the model is simulating small scales in numerical weather prediction applications, while necessarily removing energy at the gridscale but minimizing artificial dissipation at the resolved scales. Filtering requirements for atmospheric models and filters used in the ARW model are discussed.

Weather Research Model-Data Comparison (Katrina)

[*Skamarock and Klemp*, JCP, 227, 2008]

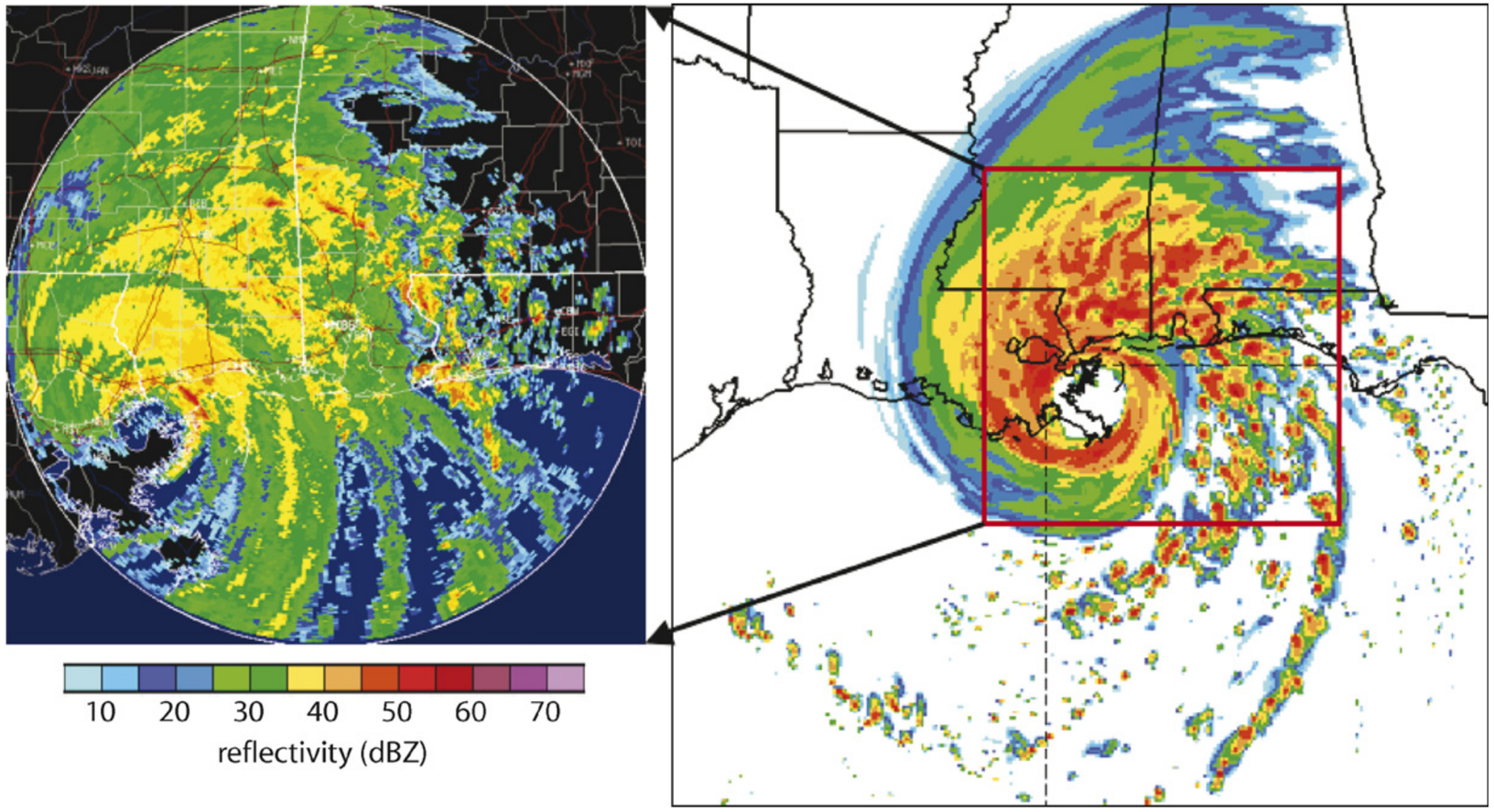

Fig. 7. Observed radar reflectivity (left) from the Mobile Alabama radar for Hurricane Katrina making landfall at 14 UTC 29 August 2005. A 62 h ARW reflectivity forecast valid at that time using $\Delta x = 4$ km.

Mesospheric concentric gravity waves generated by multiple convective storms over the North American Great Plain

Sharon Vadas,[1] Jia Yue,[2] and Takuji Nakamura[3]

Received 17 October 2011; revised 24 January 2012; accepted 22 February 2012; published 14 April 2012.

[1] We report on six continuous hours of OH airglow imager observations (at z $\sim$ 87 km) of convectively generated gravity waves (GWs) near Fort Collins, Colorado, on the evening of 08 September 2005. These GWs appeared as nearly concentric rings, and had epicenters near the locations of deep convection in three thunderstorms in Colorado, Nebraska and South Dakota. Using GOES satellite and weather radar observations, we show that the GWs closely follow the thunderstorms. Using the background wind from a nearby radar, the intrinsic wave parameters and vertical wavelengths are calculated. The temperature perturbations are estimated to be $T'/\overline{T} \sim$ 1–3% for GWs with horizontal wavelengths $\lambda_h \sim$ 20–40 km and horizontal phase speeds $\sim$40–60 m/s. The horizontal wavelengths of GWs from a convective cluster decreased in time from 30 to 15 km. We employ convective plume and ray-trace models to simulate the GW-induced OH intensity perturbations from convective plumes, clusters and complexes. We find that the results using the background model wind (radiosonde/TIME-GCM) agree well with the late-time observations, when the images are dominated by southwestward, short-wavelength, high-frequency GWs. These late-time GWs propagate against the background wind, and have $\lambda_h \sim$ 30–40 km and periods of $\tau \sim$ 20–30 min. The OH intensity perturbations are enhanced because the vertical wavelengths λ_z increased, $T'/\overline{T}$ increased, and the vertical velocity perturbations w' decreased (because the GWs were near their reflection levels). We also find that these short-wavelength GWs were created $\sim$5 h earlier by an extremely energetic, deep convective plume in South Dakota, thereby showing that small-scale, convective GWs directly link the troposphere and mesopause region.

Citation: Vadas, S., J. Yue, and T. Nakamura (2012), Mesospheric concentric gravity waves generated by multiple convective storms over the North American Great Plain, *J. Geophys. Res.*, *117*, D07113, doi:10.1029/2011JD017025.

Concentric Gravity Waves Above a Convective System

[*Vadas et al.*, JGR, 117, 2012]

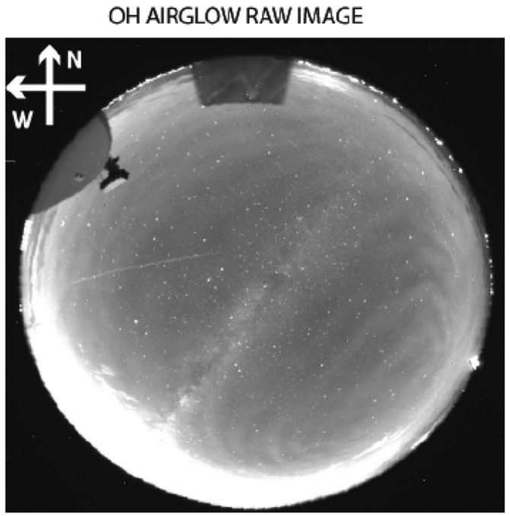

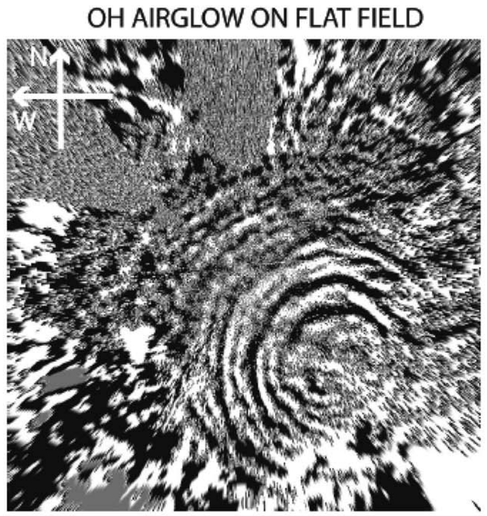

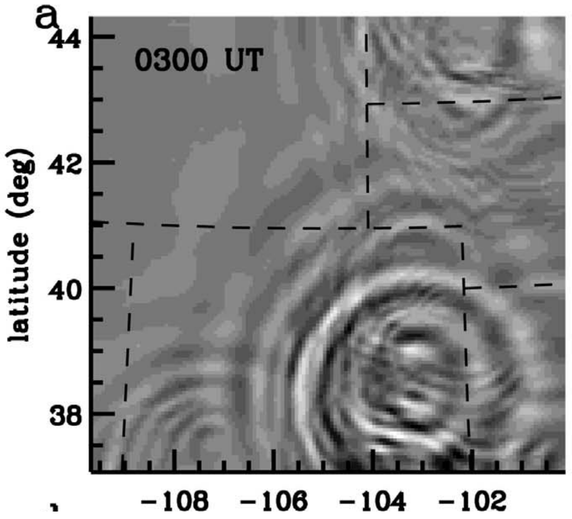

Chelyabinsk Airburst, Damage Assessment, Meteorite Recovery, and Characterization

Olga P. Popova,[1] Peter Jenniskens,[2,3]* Vacheslav Emel'yanenko,[4] Anna Kartashova,[4] Eugeny Biryukov,[5] Sergey Khaibrakhmanov,[6] Valery Shuvalov,[1] Yurij Rybnov,[1] Alexandr Dudorov,[6] Victor I. Grokhovsky,[7] Dmitry D. Badyukov,[8] Qing-Zhu Yin,[9] Peter S. Gural,[2] Jim Albers,[2] Mikael Granvik,[10] Läslo G. Evers,[11,12] Jacob Kuiper,[11] Vladimir Kharlamov,[1] Andrey Solovyov,[13] Yuri S. Rusakov,[14] Stanislav Korotkiy,[15] Ilya Serdyuk,[16] Alexander V. Korochantsev,[8] Michail Yu. Larionov,[7] Dmitry Glazachev,[1] Alexander E. Mayer,[6] Galen Gisler,[17] Sergei V. Gladkovsky,[18] Josh Wimpenny,[9] Matthew E. Sanborn,[9] Akane Yamakawa,[9] Kenneth L. Verosub,[9] Douglas J. Rowland,[19] Sarah Roeske,[9] Nicholas W. Botto,[9] Jon M. Friedrich,[20,21] Michael E. Zolensky,[22] Loan Le,[23,22] Daniel Ross,[23,22] Karen Ziegler,[24] Tomoki Nakamura,[25] Insu Ahn,[25] Jong Ik Lee,[26] Qin Zhou,[27,28] Xian-Hua Li,[28] Qiu-Li Li,[28] Yu Liu,[28] Guo-Qiang Tang,[28] Takahiro Hiroi,[29] Derek Sears,[3] Ilya A. Weinstein,[7] Alexander S. Vokhmintsev,[7] Alexei V. Ishchenko,[7] Phillipe Schmitt-Kopplin,[30,31] Norbert Hertkorn,[30] Keisuke Nagao,[32] Makiko K. Haba,[32] Mutsumi Komatsu,[33] Takashi Mikouchi,[34] (the Chelyabinsk Airburst Consortium)

The asteroid impact near the Russian city of Chelyabinsk on 15 February 2013 was the largest airburst on Earth since the 1908 Tunguska event, causing a natural disaster in an area with a population exceeding one million. Because it occurred in an era with modern consumer electronics, field sensors, and laboratory techniques, unprecedented measurements were made of the impact event and the meteoroid that caused it. Here, we document the account of what happened, as understood now, using comprehensive data obtained from astronomy, planetary science, geophysics, meteorology, meteoritics, and cosmochemistry and from social science surveys. A good understanding of the Chelyabinsk incident provides an opportunity to calibrate the event, with implications for the study of near-Earth objects and developing hazard mitigation strategies for planetary protection.

Modeled Pressure Perturbation and Glass Damage Following Chelyabinsk Meteor Event

[*Popova et al.*, Science, 342, 2013]

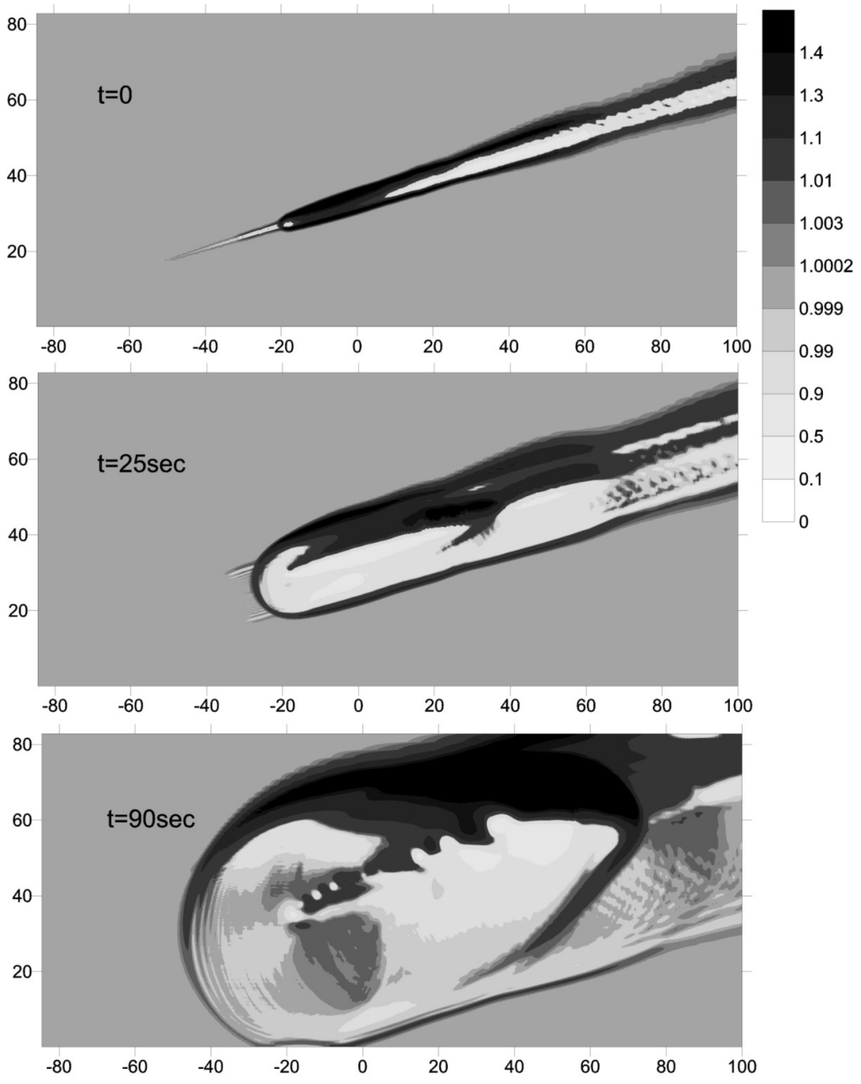

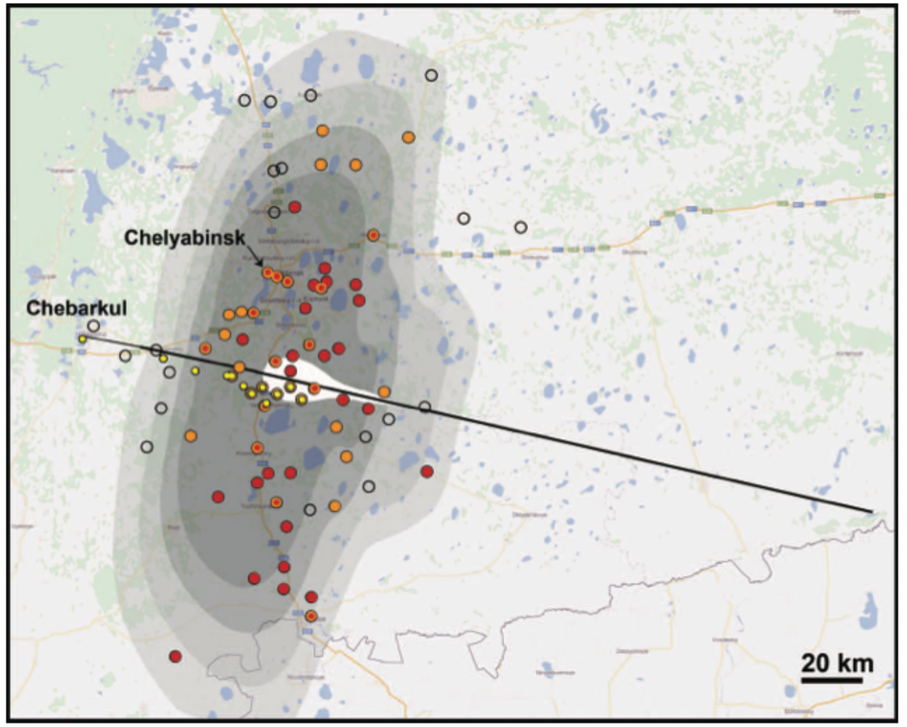

Fig. 3. Map of glass damage on the ground with models of overpressure. Field survey data are shown in solid orange circles for reported damage and open black circles for no damage; solid red circles show the most damaged villages in each district, as reported by the government. Each point, irrespective of population density, represents one of many villages or city districts scattered throughout the area. Model contours (with progressive gray scale) represent kinetic energies and overpressures from inside out: 300 kT $\Delta p > 1000$ Pa, 520 kT $\Delta p > 1000$ Pa, 300 kT $\Delta p > 500$ Pa, and 520 kT $\Delta p > 500$ Pa, respectively. Also shown are the locations of meteorite finds (yellow points) and the ground-projected fireball trajectory (black line), moving from 97-km altitude on the right to 14-km altitude on the left. White shows the fireball brightness on a linear scale.

“Tiger Elves”: Gravity Waves Illuminated by “Elve” TLEs

[*Yue and Lyons*, GRL, 2015; *Marshall et al.*, JGR, 2015]:

Structured elves: Modulation by convectively generated gravity waves

Jia Yue[1] and Walter A. Lyons[2]

[1]Department of Atmospheric and Planetary Sciences, Hampton University, Hampton, Virginia, USA, [2]FMA Research, Ft. Collins, Colorado, USA

Abstract We report on a markedly striated elve (Emissions of Light and Very Low Frequency Perturbations due to Electromagnetic Pulse Source) (a “tiger elve”) observed using an intensified high-speed Phantom camera system at the Yucca Ridge Field Station near Fort Collins, Colorado, on the night of 12 June 2013. This elve was induced by a 204 kA positive cloud-to-ground lightning flash within a mesoscale convective system in western South Dakota. A halo and a sprite followed the elve. The banded structure in the elve was aligned with convectively generated gravity waves (CGGWs) independently observed by a collocated color near-infrared camera. Assuming the height of the OH layer and elve both to be 85 km, photogrammetry allowed projection of the elve and the CGGWs onto the same geographic map. The tiger elve stripes approximately overlay on the troughs (dark bands) of CGGWs. This is consistent with model predictions that the ionization rate in the *D* region ionosphere is inversely proportional to the air density, which is modulated by the CGGWs.

Numerical simulation of an elve modulated by a gravity wave

R. A. Marshall[1,2], Jia Yue[3], and Walter A. Lyons[4]

[1]Department of Aeronautics and Astronautics, Stanford University, Stanford, California, USA, [2]Department of Aerospace Engineering Sciences, University of Colorado Boulder, Boulder, Colorado, USA, [3]Department of Atmospheric and Planetary Sciences, Hampton University, Hampton, Virginia, USA, [4]FMA Research, Fort Collins, Colorado, USA

Abstract Recent video observations have shown that elves—the visible manifestation of the lightning electromagnetic pulse (EMP) interacting with the lower ionosphere—can be modulated by neutral density fluctuations at lower ionosphere altitudes due to gravity waves. The elve emissions thus illuminate the gravity wave structure. Here we use a finite difference time domain (FDTD) model of the lightning EMP to simulate elve emissions in the presence of neutral density fluctuations representative of gravity waves. We show that observable elve striations can be generated by gravity waves with a neutral density perturbation of as low as 5% at elve altitudes near 85 km. Higher perturbations lead to more pronounced striations. The depth of the optical signature perturbation is found to be similar in magnitude to the neutral density perturbation at elve altitudes, although the relationship depends on viewing geometry, gravity wave geometry, and the elve-causative lightning peak current moment.

“Tiger Elves”:

[*Marshall et al.*, JGR, 2015]:

Elves are “airglow” triggered by lightning-generated electromagnetic pulses (EMP). Marshall et al. applied a finite-difference time-domain (FDTD) model of the EMP to a gravity-wave disturbed atmosphere to investigate the GW structures within the “Elven Airglow”.

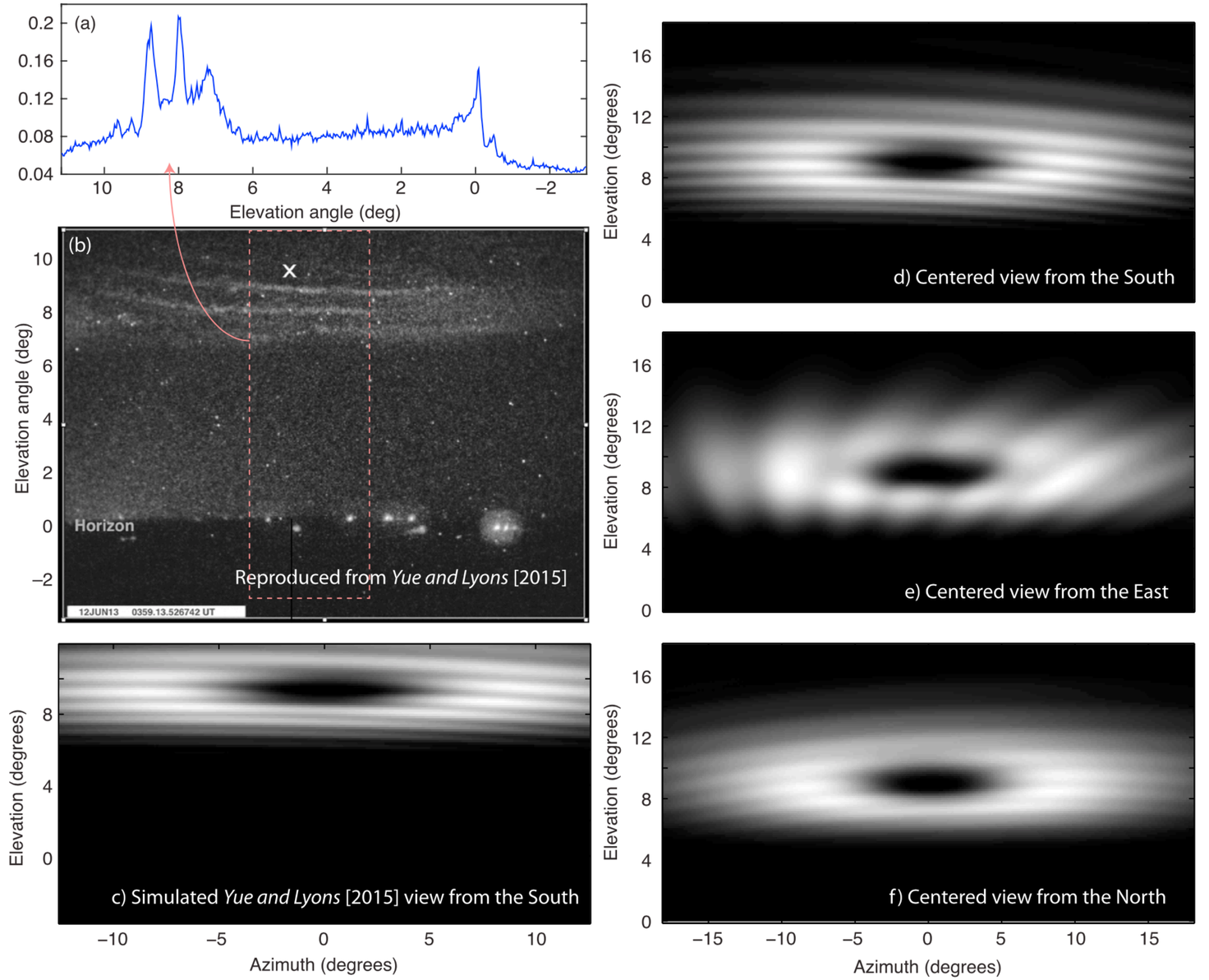

Figure 1. (top left) The elve perturbed by a GW (b) reproduced from *Yue and Lyons* [2015], as well as (a) a vertical slice in elevation. The “X” marks the point at 85 km altitude directly above the CG, which is at 9.5° elevation. The red dashed box is averaged in azimuth to produce the curve above. Note that the camera $\gamma = 1.016$, so that the response is nearly linear. (c) Simulated elve, with 20% maximum perturbation, viewed from the approximate camera field of view of the event. (right) Other simulated views of the same elve: (d) observed from the same location (south), if the camera FOV had been centered above the lightning discharge at 85 km altitude; (e) viewed from the east; or (f) viewed from the north.

Breaking Gravity Waves and Turbulence in PMCs

[*Miller, Fritts, et al.*, JGR, 2016]:

Stratospheric imaging of polar mesospheric clouds: A new window on small-scale atmospheric dynamics

A. D. Miller[1], D. C. Fritts[2], D. Chapman[1], G. Jones[1], M. Limon[1], D. Araujo[1], J. Didier[1], S. Hillbrand[3], C. B. Kjellstrand[1], A. Korotkov[4], G. Tucker[4], Y. Vinokurov[4], K. Wan[2], and L. Wang[2]

[1]Department of Physics, Columbia University, New York, New York, USA, [2]GATS Inc., Boulder, Colorado, USA, [3]Department of Physics and Astronomy, California State University, Sacramento, California, USA, [4]Department of Physics, Brown University, Providence, Rhode Island, USA

Abstract Instabilities and turbulence extending to the smallest dynamical scales play important roles in the deposition of energy and momentum by gravity waves throughout the atmosphere. However, these dynamics and their effects have been impossible to quantify to date due to lack of observational guidance. Serendipitous optical images of polar mesospheric clouds at ~82 km obtained by star cameras aboard a cosmology experiment deployed on a stratospheric balloon provide a new observational tool, revealing instability and turbulence structures extending to spatial scales < 20 m. At 82 km, this resolution provides sensitivity extending to the smallest turbulence scale not strongly influenced by viscosity: the "inner scale" of turbulence, $l_0 \sim 10(\nu^3/\epsilon)^{1/4}$. Such images represent a new window into small-scale dynamics that occur throughout the atmosphere but are impossible to observe in such detail at any other altitude. We present a sample of images revealing a range of dynamics features and employ numerical simulations that resolve these dynamics to guide our interpretation of several observed events.

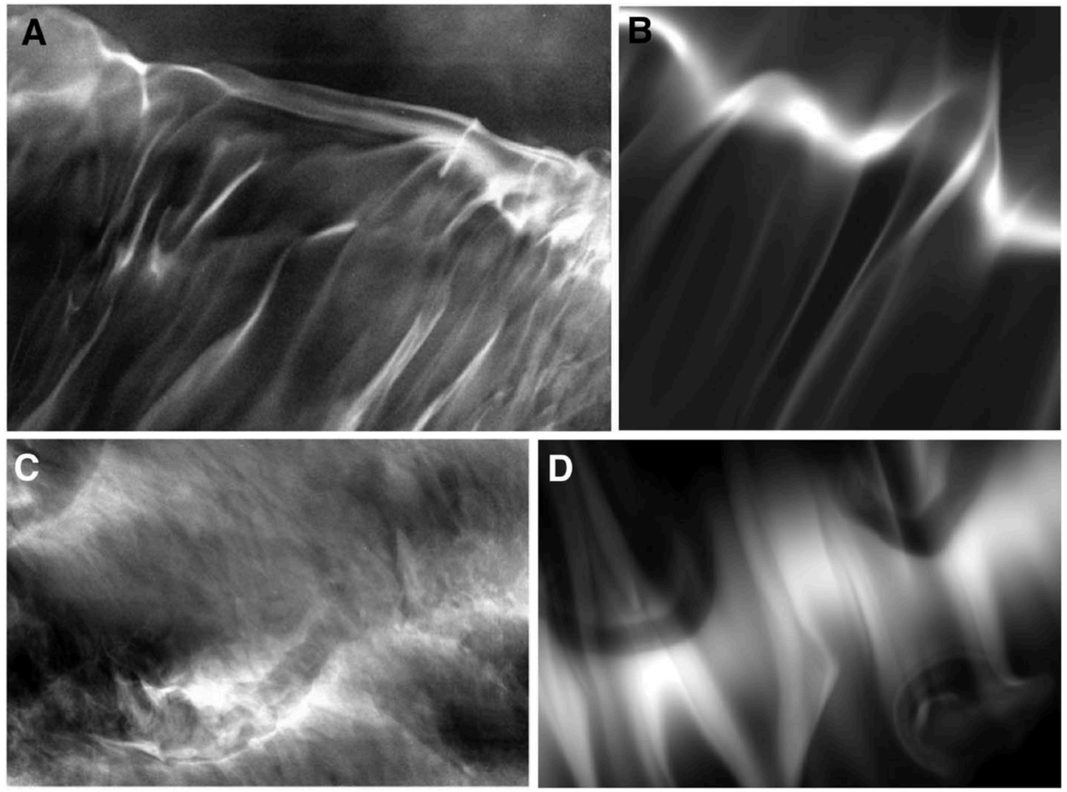

Figure 1. Comparisons of EBEX PMC images and idealized GW breaking PMC simulations. (a) An EBEX image (4.1 km × 3.3 km) of what appears to be a GW breaking front. (b) Modeled breaking GW showing a feature with the same morphology. GW propagation in each case is toward the upper right. (c) An EBEX PMC image (4.1 km × 3.3 km) exhibiting semicircular features suggestive of successive laminar vortex rings in background turbulence. (d) The corresponding result from the GW breaking simulation shows the response to true vortex rings accompanying GW breaking in a laminar background [*Fritts et al.*, 2009b].

Formation Mechanisms of Neutral Fe Layers

[*Chu and Yu*, JGR, 2017]:

Formation mechanisms of neutral Fe layers in the thermosphere at Antarctica studied with a thermosphere-ionosphere Fe/Fe$^+$ (TIFe) model

Xinzhao Chu[1]* and Zhibin Yu[1]

[1]Cooperative Institute for Research in Environmental Sciences & Department of Aerospace Engineering Sciences, University of Colorado at Boulder, 216 UCB, Boulder, CO 80309, USA

*Corresponding author: Xinzhao.Chu@Colorado.edu

Key Points:

- The first thermosphere-ionosphere Fe/Fe$^+$ (TIFe) model has been developed from first principles for Polar Regions at University of Colorado
- TIFe model formulates the TIFe theory depicting the lifecycle of meteoric metals via deposition, transport, chemistry and wave dynamics
- Antarctic lidar observations were reproduced by TIFe model via neutralization of upward-transported and wind-shear-converged Fe$^+$ layers

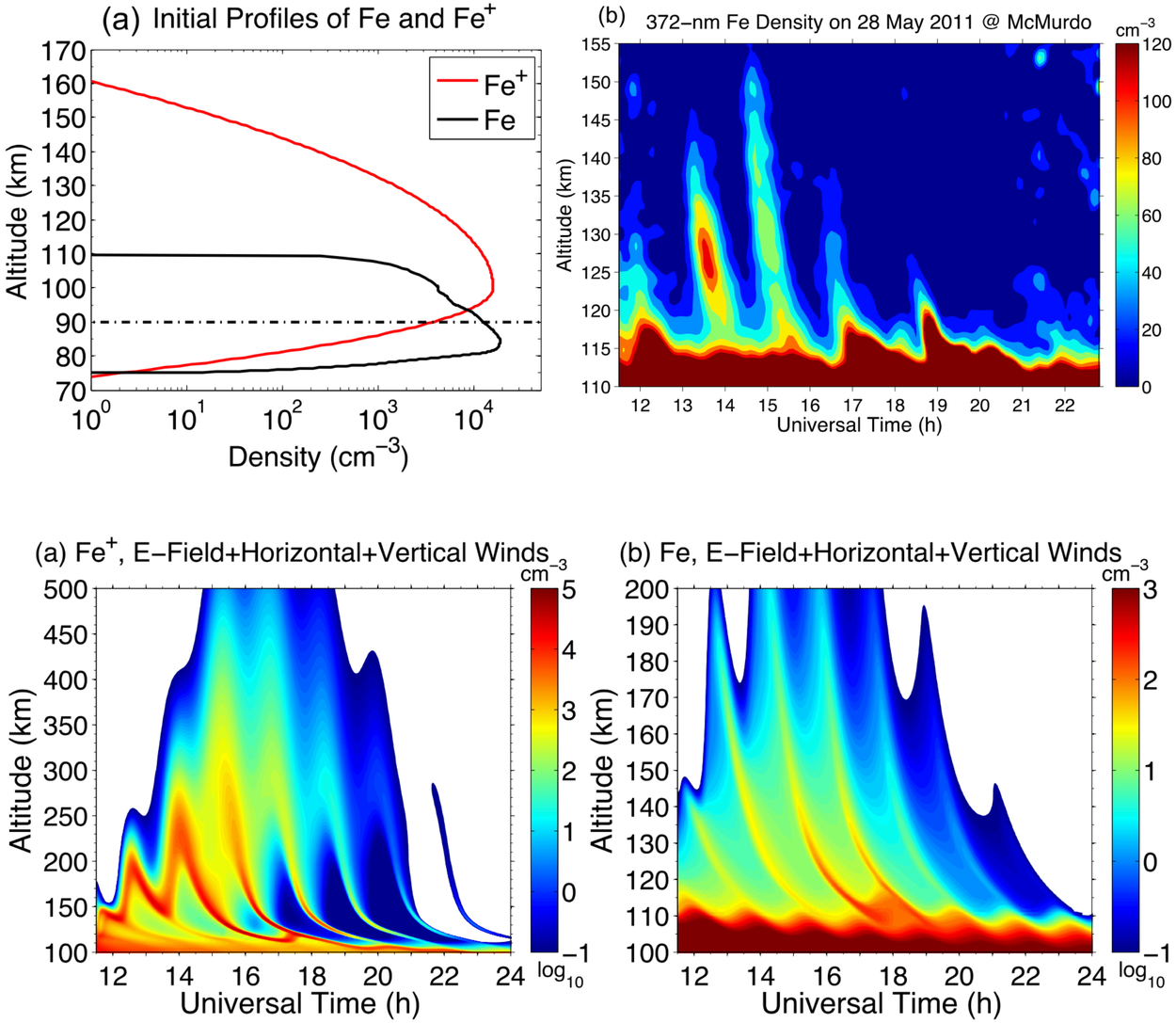

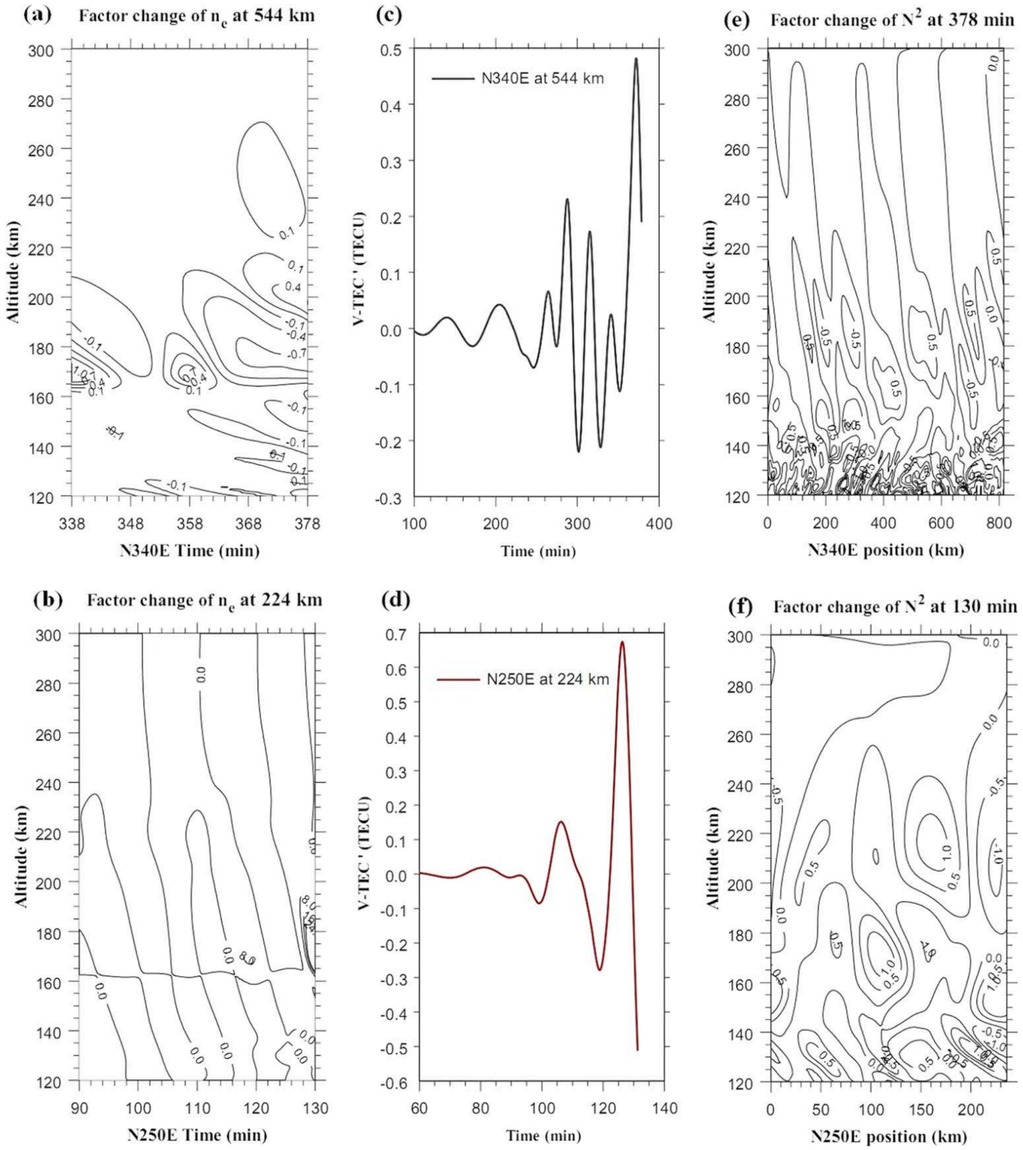

Figure 7. (a and b) Relative change of the electron number density (n_e), (c and d) time series of the V-TEC perturbations, and (e and f) relative change of the square Brunt-Väisälä frequency (N^2) due to AGWs propagating toward the N340°E (Figures 7a, 7c, and 7e) and N250°E directions (Figures 7b, 7d, and 7f) driven by the 2004 Sumatra tsunami.

AGU PUBLICATIONS

JGR

Journal of Geophysical Research: Space Physics

RESEARCH ARTICLE
10.1002/2016JA023116

Key Points:
- A 2-D nonlinear time-dependent model displays azimuthally anisotropic gravity waves driven by tsunamis shown in TEC at ionospheric heights
- Incomplete ducting conditions may cast doubt upon a long-range propagating gravity wave afar off the epicenter in the 2004 Sumatra event
- Long-range gravity wave propagation may have been overlooked in the 2011 Tohoku event owning to sparse GPS receivers in the deep Pacific

Correspondence to:
Y. Yu,
yuyong@nuaa.edu.cn

Citation:
Yu, Y., W. Wang, and M. P. Hickey (2017), Ionospheric signatures of gravity waves produced by the 2004 Sumatra and 2011 Tohoku tsunamis: A modeling study, *J. Geophys. Res. Space Physics, 122*, 1146–1162, doi:10.1002/2016JA023116.

Received 28 JUN 2016
Accepted 9 DEC 2016
Accepted article online 16 DEC 2016
Published online 24 JAN 2017

Ionospheric signatures of gravity waves produced by the 2004 Sumatra and 2011 Tohoku tsunamis: A modeling study

Yonghui Yu[1], Wenqing Wang[1], and Michael P. Hickey[2]

[1]College of Astronautics, Nanjing University of Aeronautics and Astronautics, Nanjing, China, [2]Department of Physical Sciences and Center for Space and Atmospheric Research, Embry-Riddle Aeronautical University, Daytona Beach, Florida, USA

Abstract Ionospheric fluctuations inferred from observations of total electron content have previously been attributed to tsunamis and have confirmed the strong coupling between Earth's ocean and ionosphere via atmospheric gravity waves (AGWs). To further advance our understanding of this wave coupling process we employ a linear full-wave model and a nonlinear time-dependent model to examine the ionospheric response to the AGW perturbations induced by the 2004 Sumatra and the 2011 Tohoku tsunamis. In the 2004 case, our modeling analyses reveal that one component of the propagating AGWs becomes dynamically unstable in the *E*-region ionosphere at a range exceeding 2000 km in a direction 340° clockwise from north. Another component becomes convectively unstable in the *E*-region ionosphere at a range exceeding 700 km in a direction 250° clockwise from north. In the 2011 case, a significant enhancement in the ionospheric disturbance occurs in a direction northwest from the epicenter about 1 h following the tsunami onset, in general agreement with observations. Our simulations also indicate that the AGW propagating toward the southeast is responsible for a traveling ionospheric disturbance that remains of an observable amplitude for over 4 h during which time it propagates horizontally almost 4000 km.

1. Introduction

Earthquakes often produce fast Rayleigh waves at the Earth's surface, which can in turn produce fast atmospheric acoustic waves that can propagate rapidly to ionospheric heights [e.g., *Liu et al.*, 2006, 2011]. Subterranean earthquakes are able to produce tsunamis that in turn can generate obliquely upward propagating atmospheric gravity waves (AGWs), which subsequently disturb the ionosphere thereby creating traveling ionospheric disturbances (TIDs). These can be detected by a variety of techniques, one of which is through the use of the Global Positioning System (GPS) array [e.g., *Rolland et al.*, 2010; *Galvan et al.*, 2011, 2012; *Occhipinti et al.*, 2013; *Crowley et al.*, 2016], while others utilize airglow imaging systems [*Makela et al.*, 2011; *Smith et al.*, 2015].

Lee et al. [2008] postulated that the TID observed over Arecibo on 26 December was a response to the AGW induced by the 2004 Sumatra tsunami. Shown in their Figure 7, *Lee et al.* [2008] proposed two different possible scenarios. In the first scenario, tsunami-induced AGWs propagate between Sumatra (3.316°N, 95.854°E) and Puerto Rico (18.5°N, 66°W) along a great circle path of about 18,000 km; the AGWs are imperfectly ducted for a long distance, and wave energy ultimately leaks into the ionosphere over Arecibo. In the second scenario, the AGWs over Arecibo are generated locally by nearby tsunami waves (the latter having traveled from the epicenter along a large U-turn path first across the Indian Ocean, then into the Atlantic Ocean), and propagate in the northwest direction over Arecibo.

The 2011 Tohoku tsunami occurred in an area densely distributed with a GPS array, providing an excellent opportunity to study the ionospheric response to a tsunami by monitoring the total electron content (TEC) [e.g., *Komjathy et al.*, 2012; *Galvan et al.*, 2012]. Previous tsunami-ionosphere studies have shown that the ionospheric response broadly depends on the latitude where the tsunami occurred and the direction of wave travel [e.g., *Artru et al.*, 2005a, 2005b; *Occhipinti et al.*, 2006, 2008]. *Hickey et al.* [2009] found that the ionospheric response to the 2004 Sumatra tsunami would be most favorable for tsunami propagation in the meridional direction. This dependence is due to a significant coupling between neutrals and ions that maximizes along the geomagnetic field direction near the equator [*Occhipinti et al.*, 2008].

Previous GPS observations in regions close to the epicenter have revealed that the TEC fluctuations associated with the 2011 Tohoku tsunami were largest for waves propagating toward the northwest of the

AGU PUBLICATIONS

JGR

Journal of Geophysical Research: Space Physics

RESEARCH ARTICLE
10.1002/2016JA023329

Special Section:
Inner Magnetosphere Coupling: Recent Advances

Anisotropic fluid modeling of ionospheric upflow: Effects of low-altitude anisotropy and thermospheric winds

M. Burleigh[1] and M. Zettergren[1,2]

[1]Department of Physical Sciences and Center for Space an Atmospheric Research, Embry-Riddle Aeronautical University, Daytona Beach, Florida, USA, [2]Center for Space Physics Boston University, Boston, Massachusetts, USA

Key Points:
- A new anisotropic fluid model is developed and describes ionospheric responses to energy sources causing anisotropy
- DC electric fields dominate temperature anisotropies at lower altitudes, while wave heating dominates at higher altitudes
- High-latitude thermospheric winds can aid or hinder upflow depending on the wind direction

Correspondence to:
M. Burleigh,
burleb34@my.erau.edu

Citation:
Burleigh, M., and M. Zettergren (2017), Anisotropic fluid modeling of ionospheric upflow: Effects of low-altitude anisotropy and thermospheric winds, *J. Geophys. Res. Space Physics, 122*, 808–827, doi:10.1002/2016JA023329.

Received 13 AUG 2016
Accepted 29 NOV 2016
Accepted article online 7 DEC 2016
Published online 3 JAN 2017

Abstract A new anisotropic fluid model is developed to describe ionospheric upflow responses to magnetospheric forcing by electric fields and broadband ELF waves at altitudes of 90–2500 km. This model is based on a bi-Maxwellian ion distribution and solves time-dependent, nonlinear equations of conservation of mass, momentum, parallel energy, and perpendicular energy for six ion species important to *E*, *F*, and topside ionospheric regions. It includes chemical and collisional interactions with the neutral atmosphere, photoionization, and electron impact ionization. This model is used to examine differences between isotropic and anisotropic descriptions of ionospheric upflow driven by DC electric fields, possible effects of low-altitude (<500 km) wave heating, and impacts of neutral winds on ion upflow. Results indicate that isotropic models may overestimate field-aligned ion velocity responses by as much as ~48%. Simulations also show significant ionospheric responses at low altitudes to wave heating for very large power spectral densities, but ion temperature anisotropies below the *F* region peak are dominated by frictional heating from DC electric fields. Neutral winds are shown to play an important role regulating ion upflow. Thermospheric winds can enhance or suppress upward fluxes driven by DC and BBELF fields by 10–20% for the cases examined. The time history of the neutral winds also affects the amount of ionization transported to higher altitudes by DC electric fields.

1. Introduction

Ion production, loss, and transport in the high-latitude *F* region ionosphere are regulated by electric fields and auroral precipitation, both of which can lead to strong thermal plasma upflow. Frictional heating-driven upflow (type 1 of *Wahlund et al.* [1992]) events are typically associated with elevated ion temperatures, strong convection electric fields, and minimal auroral precipitation. In these events, strong convection of the ionosphere through the neutral atmosphere leads to frictional heating of the ions in the *E* and *F* regions of the ionosphere, resulting in anisotropic ion distributions [*St-Maurice and Schunk*, 1979] and large pressure gradients that accelerate ions upward along the field lines [*Foster et al.*, 1998; *Zettergren and Semeter*, 2012]. Observations of frictional heating-driven upflows often show a lifted *F* region peak location, low electron densities below 300 km, and modest increases in electron temperature [*Wahlund et al.*, 1992]. In contrast, electron heating-driven upflow (type 2 of *Wahlund et al.* [1992]) events are associated with auroral precipitation that increases electron densities and temperatures, hence pressure, throughout the *F* region and topside ionosphere. The electron pressure increase results in a stronger ambipolar electric field which enhances the upward field-aligned flow of plasma. Electron heating-driven upflows are found above auroral arcs, seem to occur more often, and are usually stronger than frictional heating-driven upflows [*Foster and Lester*, 1996; *Wahlund et al.*, 1992; *Ogawa et al.*, 2003]. Thermal ion upflow mechanisms may not be strong enough to accelerate ions to escape velocities but instead are thought to provide source populations for higher-altitude energization processes. Once ions have been lifted to high altitudes, transverse ion acceleration by broadband ELF waves may give the upflowing ions sufficient energy, which can be converted into parallel momentum through the mirror force, to outflow into the magnetosphere [*Kintner et al.*, 1996; *Andre et al.*, 1998; *Moore et al.*, 1999]. The existence of a multistep process resulting in ionospheric outflow is supported by observations of concurrent ion upflow and outflow drivers (fields, precipitation, ELF waves, etc.) [*Yoshida et al.*, 1999; *Lynch et al.*, 2007; *Ogawa et al.*, 2008; *Strangeway et al.*, 2005].

A variety of modeling studies have established many of the general characteristics of electron heating-driven upflows and outflows driven by auroral processes. The Dynamic Fluid-Kinetic model (DyFK) [*Wu et al.*, 1999] is

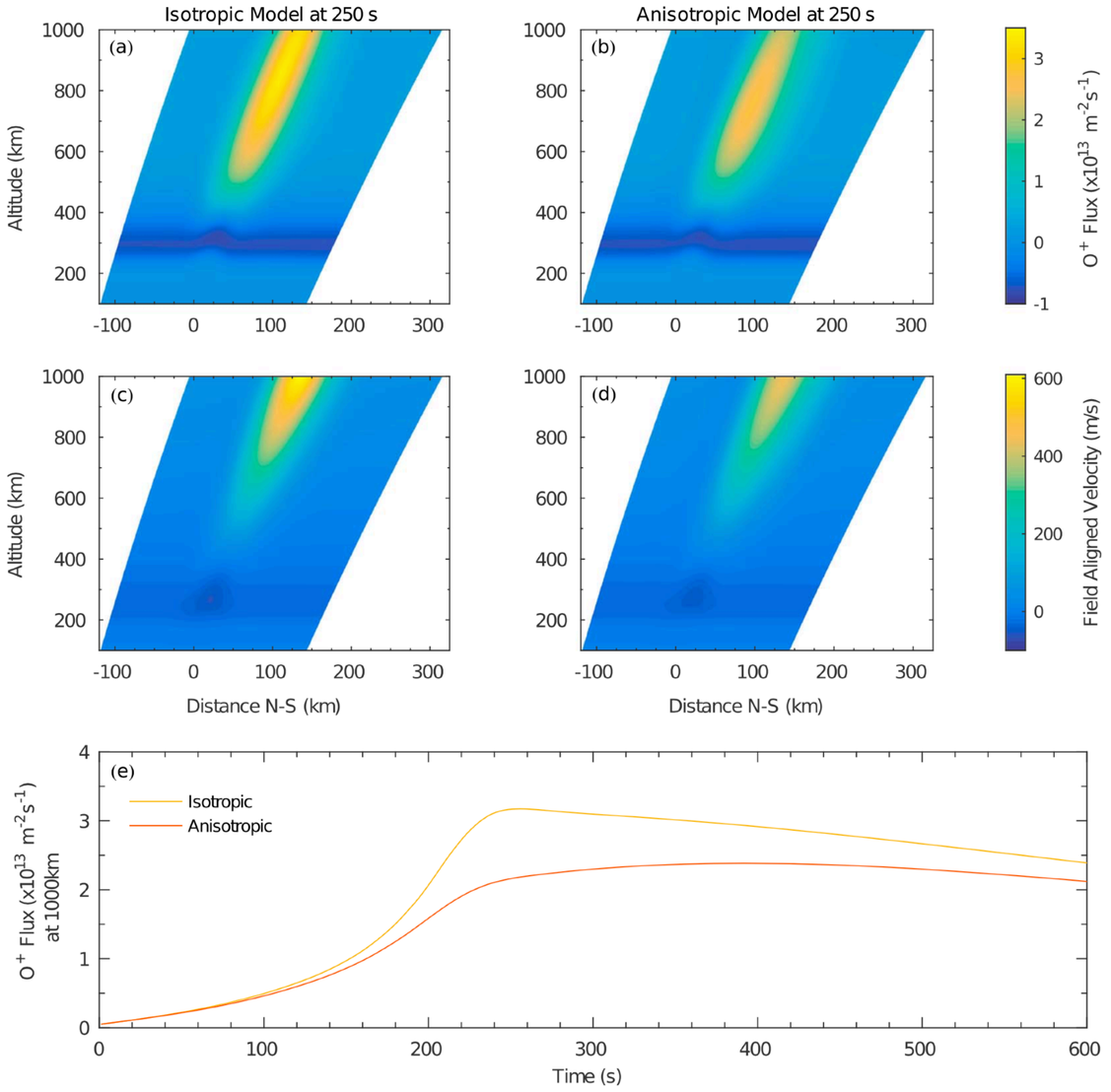

Figure 1. A comparison of the O^+ flux and field-aligned velocity between the new 16-moment (anisotropic) model and the parent 5-moment (isotropic) model after 250 s of an applied DC electric field of 80 mV/m. (a) Isotropic O^+ flux, (b) anisotropic O^+ flux, (c) isotropic field-aligned velocity, (d) anisotropic field-aligned velocity, and (e) both the isotropic and anisotropic O^+ flux at 1000 km, on the center field line of the simulation, for the entire duration of the simulation. There is a significantly larger response in the isotropic model compared to the anisotropic model, 48% larger at 250 s at 1000 km. The field-aligned velocity is also larger with a 33% increase in the isotropic velocity response when compared to the anisotropic response. Figure 1e highlights the consistency of the isotropic flux response to be larger than the anisotropic flux response.

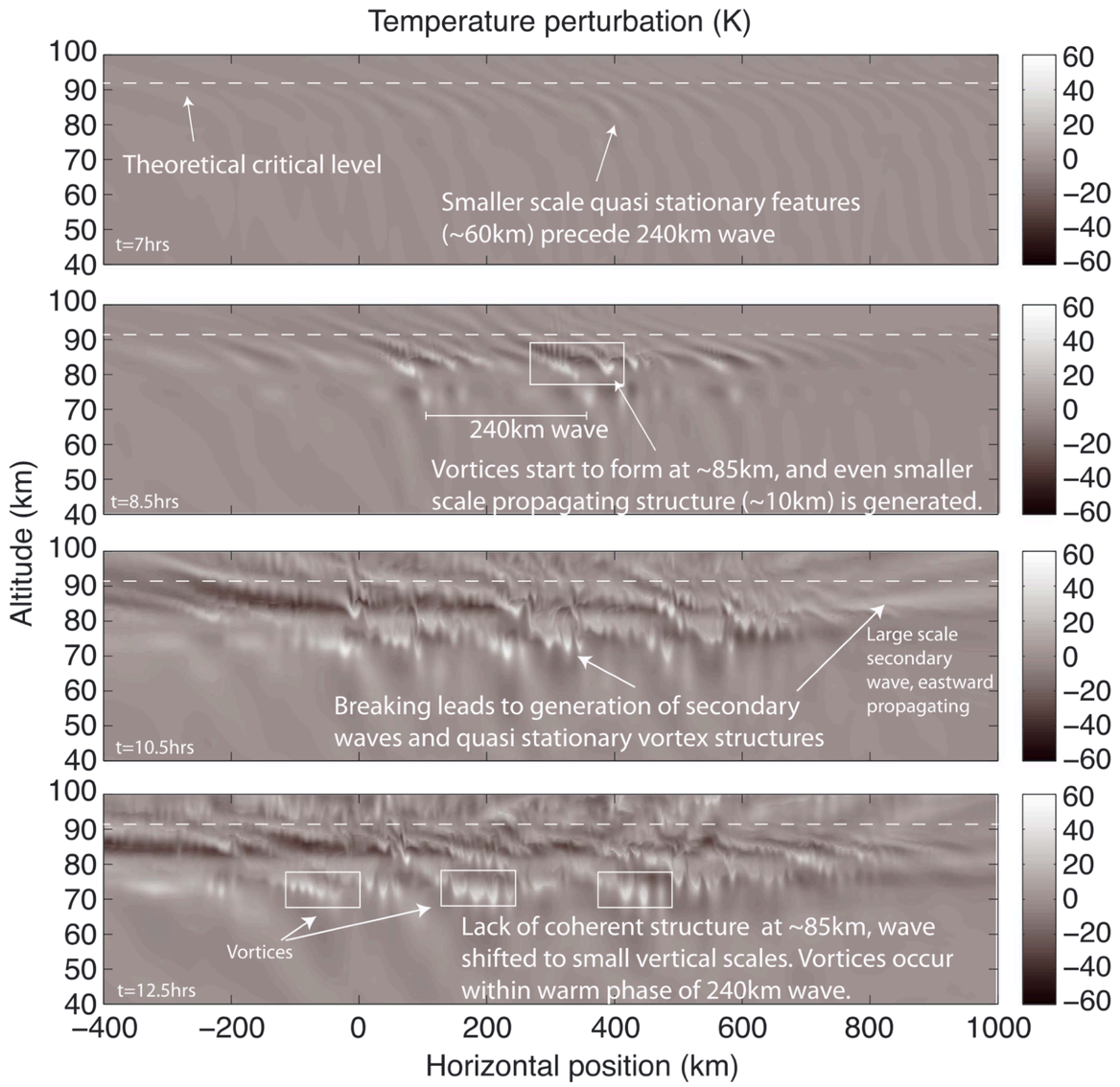

Figure 3. The simulation of the RF22 event, showing the perturbation temperature at four different times. The simulation shows the onset of breaking which creates 10km scale propagating structure initially. As time progresses, stationary vortex structures form as well as large and small-scale secondary features which propagate both eastward and westward. It becomes unclear at late times what features are actually a wave and what are instability feature that advect with the wave/background wind.

AGU PUBLICATIONS

JGR

Journal of Geophysical Research: Atmospheres

RESEARCH ARTICLE
10.1002/2016JD025700

Key Points:
- A 2-D nonlinear, compressible model is used to investigate a large-amplitude, multiscale mountain wave event
- Small-scale waves and vortices are generated in situ by a breaking mountain wave, consistent with observations
- There is a preference for instability to appear most prominent in the warm phase front of the mountain wave

Correspondence to:
C. J. Heale,
healec@erau.edu

Citation:
Heale, C. J., K. Bossert, J. B. Snively, D. C. Fritts, P.-D. Pautet, and M. J. Taylor (2017), Numerical modeling of a multiscale gravity wave event and its airglow signatures over Mount Cook, New Zealand, during the DEEPWAVE campaign, *J. Geophys. Res. Atmos.*, *122*, 846–860, doi:10.1002/2016JD025700.

Received 25 JUL 2016
Accepted 5 JAN 2017
Accepted article online 9 JAN 2017
Published online 27 JAN 2017

Numerical modeling of a multiscale gravity wave event and its airglow signatures over Mount Cook, New Zealand, during the DEEPWAVE campaign

C. J. Heale[1], K. Bossert[2], J. B. Snively[1], D. C. Fritts[2], P.-D. Pautet[3], and M. J. Taylor[3]

[1]Department of Physical Sciences, Embry-Riddle Aeronautical University, Daytona Beach, Florida, USA, [2]GATS Inc., Boulder, Colorado, USA, [3]Center for Atmospheric and Space Sciences, Utah State University, Logan, Utah, USA

Abstract A 2-D nonlinear compressible model is used to simulate a large-amplitude, multiscale mountain wave event over Mount Cook, NZ, observed as part of the Deep Propagating Gravity Wave Experiment (DEEPWAVE) campaign and to investigate its observable signatures in the hydroxyl (OH) layer. The campaign observed the presence of a λ_x = 200 km mountain wave as part of the 22nd research flight with amplitudes of >20 K in the upper stratosphere that decayed rapidly at airglow heights. Advanced Mesospheric Temperature Mapper (AMTM) showed the presence of small-scale (25–28 km) waves within the warm phase of the large mountain wave. The simulation results show rapid breaking above 70 km altitude, with the preferential formation of almost-stationary vortical instabilities within the warm phase front of the mountain wave. An OH airglow model is used to identify the presence of small-scale wave-like structures generated in situ by the breaking of the mountain wave that are consistent with those seen in the observations. While it is easy to interpret these feature as waves in OH airglow data, a considerable fraction of the features are in fact instabilities and vortex structures. Simulations suggest that a combination of a large westward perturbation velocity and shear, in combination with strong perturbation temperature gradients, causes both dynamic and convective instability conditions to be met particularly where the wave wind is maximized and the temperature gradient is simultaneously minimized. This leads to the inevitable breaking and subsequent generation of smaller-scale waves and instabilities which appear most prominent within the warm phase front of the mountain wave.

1. Introduction

Gravity waves are understood to play a crucial role in the transfer of energy and momentum from lower atmospheric sources to the mesosphere and lower thermosphere (MLT) region [*Hung and Kuo*, 1978; *Lindzen*, 1981; *Holton*, 1982; *Vincent and Reid*, 1983; *Fritts and Dunkerton*, 1985; *Fritts and Vincent*, 1987; *Kelley*, 1997; *Hocke and Tsuda*, 2001; *Fritts and Alexander*, 2003]. Air flow over topography and convective processes such as thunderstorms, weather fronts, and shears provide efficient sources for gravity wave generation [*Fritts and Alexander*, 2003, and references cited within]. Through physical mechanisms such as breaking, dissipation, and critical level filtering, gravity waves have the ability to cause momentum and energy deposition into the upper atmosphere and influence mean temperatures and winds [*Pitteway and Hines*, 1963; *Lindzen*, 1981; *Holton*, 1982, 1983; *Fritts*, 1984; *Fritts et al.*, 1996, 2006; *Vadas and Fritts*, 2006; *Vadas*, 2007; *Yiğit et al.*, 2008, 2009; *Vadas and Liu*, 2009; *Fritts and Lund*, 2011; *Waterscheid and Hickey*, 2011; *Hickey et al.*, 2011; *Vadas and Liu*, 2013; *Heale et al.*, 2014a, 2014b]. One such manifestation of this is the reversal of the mesospheric jets and the cold summer mesopause [*Lindzen*, 1981; *Holton*, 1982, 1983; *Garcia and Solomon*, 1985; *Lübken et al.*, 1999; *Fritts and Alexander*, 2003; *Fritts et al.*, 2006]; thus, understanding the effects of gravity waves on the MLT is necessary for more accurate general circulation models and predictions.

Numerous studies have been performed to quantify the momentum flux due to gravity waves [*Fritts and Vincent*, 1987; *Tsuda et al.*, 1990; *Hitchman et al.*, 1992; *Nakamura et al.*, 1993; *Fritts and Lu*, 1993; *Swenson et al.*, 1999; *Espy et al.*, 2006; *Gardner and Liu*, 2007], and many suggest that small-scale waves (10–100 km wavelength) with high phase speeds are likely to have the largest influences in the MLT region [*Vincent and Reid*, 1983; *Fritts and Vincent*, 1987; *Fritts et al.*, 2014]. However, large-amplitude gravity waves can cascade into other scales [e.g., *Klostermeyer*, 1991; *Fritts et al.*, 2009; *Lund and Fritts*, 2012], and it can be unclear in airglow and

AGU PUBLICATIONS

Geophysical Research Letters

RESEARCH LETTER
10.1002/2017GL075360

Nonlinear Gravity Wave Forcing as a Source of Acoustic Waves in the Mesosphere, Thermosphere, and Ionosphere

J. B. Snively[1]

[1]Department of Physical Sciences, Embry-Riddle Aeronautical University, Daytona Beach, FL, USA

Key Points:
- Strong gravity waves (GWs) exhibit nonlinear fluxes of vertical momentum
- Nonlinear GW fluxes may force harmonic acoustic waves (AWs)
- AWs may be detectable above interacting GW fields and overturning regions

Supporting Information:
- Supporting Information S1

Correspondence to:
J. B. Snively,
snivelyj@erau.edu

Citation:
Snively, J. B. (2017). Nonlinear gravity wave forcing as a source of acoustic waves in the mesosphere, thermosphere, and ionosphere. *Geophysical Research Letters*, *44*. https://doi.org/10.1002/2017GL075360

Received 17 AUG 2017
Accepted 30 OCT 2017
Accepted article online 6 NOV 2017

Abstract Numerical simulations demonstrate theoretical predictions that gravity waves with short periods (~4–8 min) in the mesosphere and lower thermosphere may force secondary acoustic waves, with harmonic periods (~2-4 minutes), that can reach detectable amplitudes in the thermosphere and ionosphere. The mechanism is through their vertical fluxes of vertical momentum, which lead to forcing as they are disrupted by varying stratification or instability. This is shown likely to occur where horizontally or radially opposing gravity waves interact at large amplitudes, such as above large convective sources, and after overturning. Evanescence and reflection of the waves can lead to further enhancements of the vertical fluxes and the potential for forcing. Results thus identify one of likely several mechanisms for the nonlinear conversion from gravity waves to acoustic waves, to elucidate an unappreciated source of vertical coupling.

1. Introduction

Acoustic waves (AWs) in the ionosphere, thermosphere, and mesosphere (ITM) above convection, while observed for decades (e.g., Georges, 1973), have recently received new attention as their perturbations can be mapped in Global Positioning System (GPS) total electron content (TEC) data (e.g., Nishioka et al., 2013). The AWs in data, with periods ~1–4 min, are often accompanied by detectable gravity waves (GWs) at greater radii (e.g., Lay et al., 2015), typically with periods of ~6–30 min. Both AWs and GWs, such as reported by Nishioka et al. (2013), are often observed to persist over long periods of time (hours), likely due to reflection and ducting in addition to the persistence of forcing.

Tropospheric convective disturbances may impose thermal and mechanical forcing over short periods, leading to the generation of upward propagating AWs and GWs (e.g., Walterscheid et al., 2003; Vadas, 2013). These waves may become trapped below the lower thermosphere, thus forming resonances or ducted modes, while gradually leaking upward into the thermosphere-ionosphere. This provides a simple explanation for their observed persistence following seismic events and severe weather (e.g., Matsumura et al., 2012; Nishioka et al., 2013, and references therein). Modeled "updraft" sources, used to demonstrate primary AW and GW observability in the mesospheric hydroxyl airglow by Snively (2013) and ionospheric TEC by Zettergren and Snively (2013), also excite resonant AWs and GWs similar to those reported in thermospheric observations. In addition to filtering via reflection and resonance, the spectral coherence of AWs is enhanced by viscous dissipation and the vertical integration of TEC measurements, which typically limits the observable bandpass to periods longer than 1 min (Zettergren & Snively, 2015).

Model simulations of Zettergren et al. (2017) support that reflection and resonance processes enhance persistence of AW signatures, especially above larger (more directive) source regions. Indeed, observations reveal correlations between AW occurrences and larger source spatial scales (Lay et al., 2015). Shao and Lay (2016) also found that AWs correlate with convective downdrafts and stratiform regions that may be offset from the most active convection. This also suggests correlation with electric discharge events in the troposphere and above (e.g., Pasko, 2009; de Larquier & Pasko, 2010), although it is unclear whether these fast processes couple well to the ~1–4 min period AWs detected.

Here a simple nonlinear mechanism is demonstrated for the generation of acoustic waves, which may be either transient or persistent, via nonlinearity of gravity waves especially as they interact or overturn. By this mechanism, AWs are generated with periods ~2–4 min, consistent with harmonics of GWs with periods of ~4–8 min (or longer, when GWs break/cascade to smaller scales and shorter periods while retaining sufficient coherence). The mathematical and physical basis for these investigations is well established from

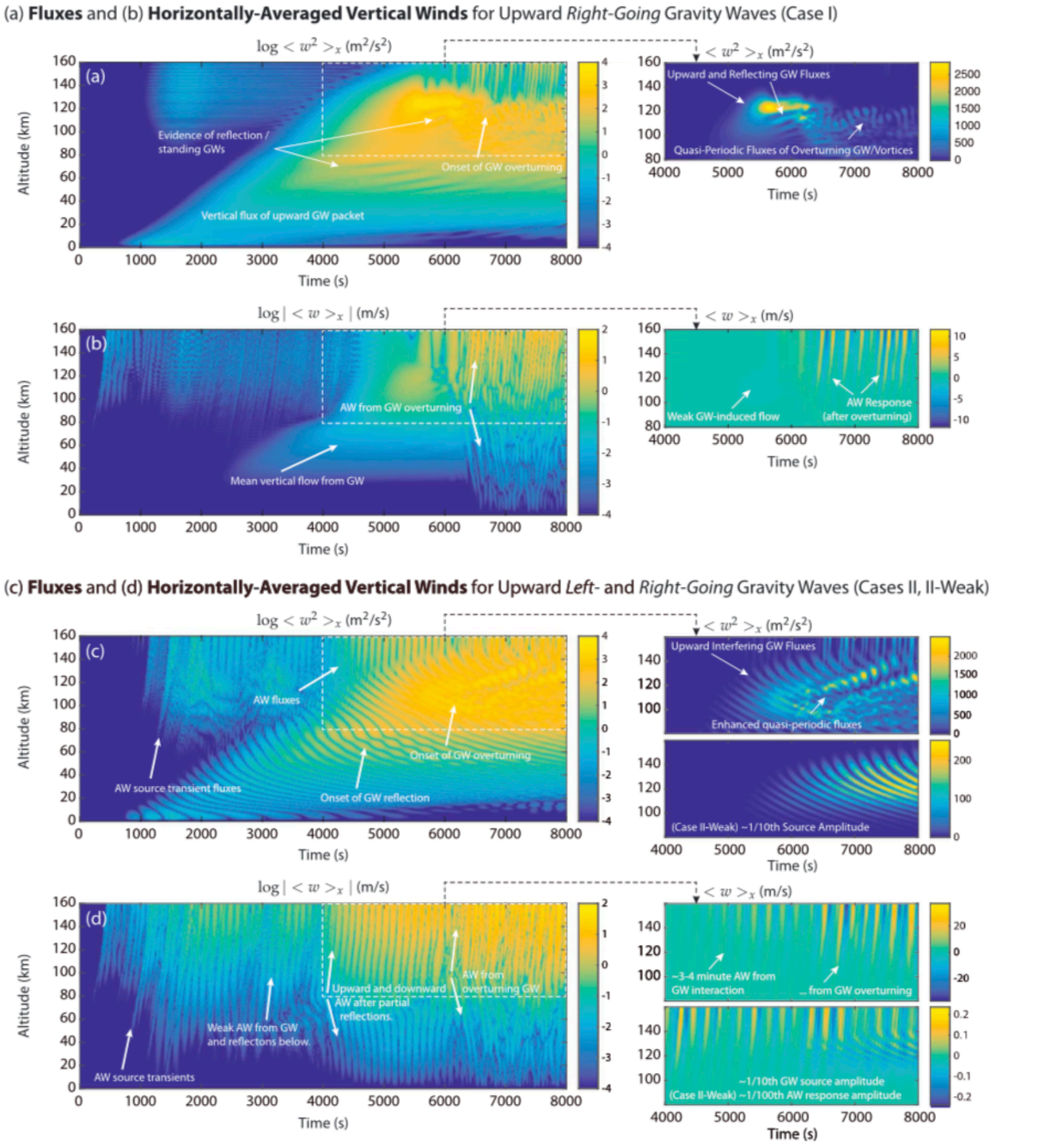

Figure 2. Time evolutions of horizontally averaged (a, c) vertical fluxes and (b, d) wind magnitudes for Case I (right-going) and Case II (left- and right-going) gravity waves, plotted on log scales, with subpanels (on right side) showing isolated data plotted on linear scales. Subpanels are included for Case II-Weak (for one tenth source amplitude of Case II), revealing the quadratic amplitude relationship between primary GWs and secondary AWs.

Summary / Conclusions

Summary / Conclusions

- Modeling is an important and, indeed, necessary methodology, complementary to experiment and theory;

Summary / Conclusions

- Modeling is an important and, indeed, necessary methodology, complementary to experiment and theory;

- models are key products of our experimental science;

Summary / Conclusions

- Modeling is an important and, indeed, necessary methodology, complementary to experiment and theory;
- models are key products of our experimental science;
- simulations are experiments that you perform with models, which can guide new experiments in reality.

Summary / Conclusions

- Modeling is an important and, indeed, necessary methodology, complementary to experiment and theory;
- models are key products of our experimental science;
- simulations are experiments that you perform with models, which can guide new experiments in reality.
- Our “Little” / “Cute” / “Idealized” / “Toy” models are often a critical first step towards new scientific understanding, and/or may provide building blocks for “Large” / “Realistic” / “Operational” models of the future.